PHYS 574

Particle Detectors

Douglas M. Gingrich

December 7, 2011

Contents

Preface

The operation of a detector that measures particles depends on the way in which the particles interact with the materials of the detector. A familiarity with the fundamental mechanisms of energy loss by particles in matter is thus essential to the understanding of the response of any particle detector.

We will first study the passage of particles though matter and then discuss calorimeter detectors. We will concentrate on sampling calorimeters and study the basic underlying principles of designing such generic detectors. Specific sampling calorimeters used in past, current, and future detector system will be left for self-study by the student.

Chapter 1

Passage of Particles Through Matter

Particles can be divided into two types depending on if they are subject to electromagnetic interactions or not. The only particle, that we will consider, that is not subjected to electromagnetic interactions is the neutron. For the neutron, processes involving the strong interaction will dominate. Neutrinos only interact weakly and normally pass through matter leaving no energy. Thus their interaction with matter will not be discussed here. The particles that interact electromagnetically include charged heavy particles of mass comparable with the nuclear mass, muons, electrons and positron, and photons. For charged particles and photons, the most common processes are electromagnetic interactions. For muons and electrons[1], only electromagnetic interactions are important. For protons and heavier particles, nuclear interactions can also be important.

Two principle features characterise the passage of charged particles through matter are

1. loss of the particle's energy and
2. deflection of the particle from its incident direction.

These effects are primarily the result of two processes:

1. inelastic collisions with the atomic electrons of the material and
2. elastic scattering from the atomic nuclei of the material.

Elastic scattering occurs from both the atomic nuclei and atomic electrons but most often from the atomic electrons. Atomic electrons are responsible for about 4 000 times more energy loss than the nuclei. In general, very little energy is transferred in these collisions since the masses of the nuclei of most materials are usually large compared to the incident particle.

Since radiation processes depend on the mass of the particle relative to the mass of the atomic electrons, it is beneficial to separate charged particles into two classes:

[1]Electrons and positrons have similar electromagnetic interactions in matter. Most of the statements we will make about electrons apply equally well to positrons.

1. heavy particles (heavier than the electron), and

2. electrons and positrons.

The former group includes muons, pions, protons, alpha particles, and other light nuclei. We now discuss each class of charged particles in turn.

1.1 Energy Loss of Heavy Charged Particles

Of the two electromagnetic processes, the inelastic collision are almost solely responsible for the energy loss of heavy particles in matter. In these collisions energy is transfered from the particle to the atom causing an ionisation or excitation of the atom. The amount of energy transferred in each collision is generally a very small fraction of the particle's total kinetic energy. The maximum energy that can be transferred from a charged particle of mass m with kinetic energy E to an electron of mass m_e in a single collision is $4Em_e/m$, or about 1/500 of the particle energy for protons. However, in normal dense matter, the number of collisions per unit path length is so large, that a substantial cumulative energy loss is observed even in relatively thin layers of material. These atomic collisions are customarily divided into two groups:

1. soft collisions in which only an excitation results and (The energy transfer is sufficient to raise the electron to a higher-lying shell within the absorber atom.)

2. hard collisions in which the energy transferred is sufficient to cause ionisation. (The energy transfer is sufficient to remove completely the electron from the atom.)

In some of the hard reactions, enough energy is transferred such that the ionised electron itself causes substantial secondary ionisation. These high-energy recoil electrons are sometimes referred to as delta-ray or knock-on electrons. Under typical conditions, the majority of the energy loss of the charge particle occurs via these delta rays. The range of the delta rays is always very small compared with the range of the incident charge particle, and in most practical situation it is immaterial whether the energy is deposited directly by the primary particle itself or by the secondary delta rays.

The inelastic collisions are statistical in nature, occurring with a certain quantum mechanical probability. However, because their number per macroscopic path length is generally large, the fluctuations in the total energy loss are small and one can meaningfully work with the average energy loss per unit path length. This qunaity is often called the linear stopping power or simply dE/dx. The value of $-dE/dx$ along a particle track is called its specific energy loss, or its rate of energy loss. Figure 1.1 shows the stopping power for muons in copper.

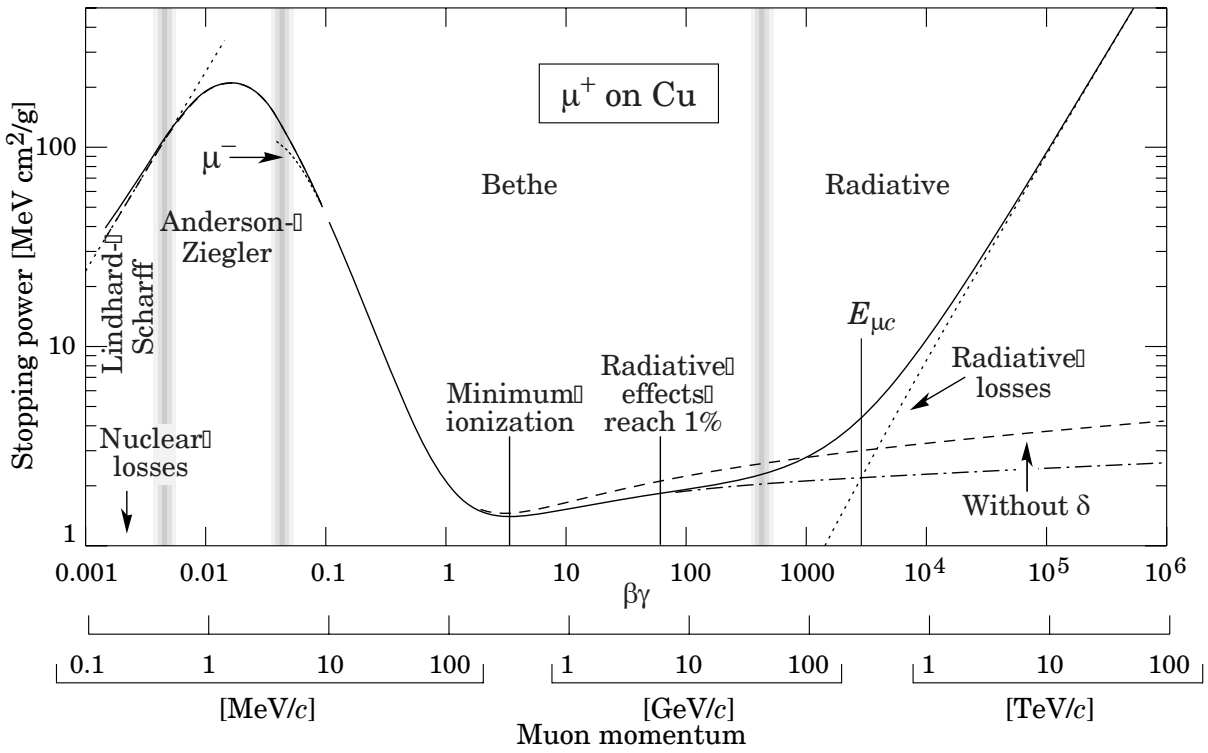

Figure 1.1: Stopping power ($= \langle -dE/dx \rangle$) for positive muons in copper as a function of $\beta\gamma = p/(Mc)$ over nine orders of magnitude in momentum (12 orders of magnitude in kinetic energy). Solid curves indicate the total stopping power. Vertical bands indicate boundaries between different approximations. The short dotted lines labelled "μ^-" illustrate the Barkas effect, the dependence of stopping power on projectile charge at very low energies. [PDG]

1.1.1 Bethe-Bloch Formula

Consider the kinetic energy loss of a charged particle due to its Coulomb interaction with a charge particle of matter. The result for the mean energy loss, or stopping power, of a heavy, spin-0 incident particle is

$$-\left\langle \frac{dE}{dx} \right\rangle = 4\pi N_A e^2 z^2 \frac{Z}{A} \frac{1}{\beta^2} \left(\frac{1}{2} \ln \frac{2m_e c^2 \beta^2 \gamma^2 T_{\max}}{I^2} - \beta^2 \right) . \tag{1.1}$$

where N_A is Avogadro's number, ze is the charge of the incident particle, Z is the atomic number of the absorbing material, A is the atomic mass of the absorbing material, m_e is the electron mass, I is the mean excitation energy, $T_{\max}$ is the maximum energy transfer in a single collision. If A is in units of g mol^{-1}, then dE/dx will be in units of MeV g^{-1} cm^2. The corresponding formula for spin-1/2 particles differs from this, but in practice the differences are small and may be neglected when discussing the main features of ionisation energy loss.

It is common practice to divide the stopping power formula Eq. (1.1) by the mass density

ρ and to redefine x as the density multiplied by the distance travelled, so that x is now measured in g cm^{-2}. If the density ρ multiplies the above expression, x is a distance rather than a mass thickness.

The maximum energy transfer is that produced by a head-on or knock-on collision. For an incident particle of mass M, kinematics gives

$$T_{\max} = \frac{2m_e c^2 \beta^2 \gamma^2}{1 + 2\gamma m_e/M + (m_e/M)^2}\,, \tag{1.2}$$

For $M \gg m_e$,

$$T_{\max} \approx 2m_c c^2 \gamma^2 \beta^2 \tag{1.3}$$

and

$$-\left\langle \frac{dE}{dx} \right\rangle = 4\pi N_A e^2 z^2 \frac{Z}{A} \frac{1}{\beta^2} \left(\ln \frac{2m_e c^2 \beta^2 \gamma^2}{I} - \beta^2 \right). \tag{1.4}$$

For all practical purposes in high-energy physics dE/dx in a given material depends only on β, except for a minor dependence on M, through $T_{\max}$, at the highest energies.

It is beneficial to separate the factors in front of the Eq. (1.4) into separate factors relating to the incident particle, the material medium, and the intrinsic properties of the electron. Using the classical radius of electron

$$r_e = \frac{e^2}{m_e c^2} = 2.8 \text{ fm} \tag{1.5}$$

and defining the constant

$$K = 4\pi N_A r_e^2 m_e c^2\,, \tag{1.6}$$

we obtain

$$-\left\langle \frac{dE}{dx} \right\rangle = K \frac{Z}{A} \frac{z^2}{\beta^2} \left(\ln \frac{2m_e c^2 \beta^2 \gamma^2}{I} - \beta^2 \right). \tag{1.7}$$

The magnitude of the energy loss depends on the medium. The electron density is given by $n_e = \rho N_A Z/A$, where ρ is the mass density of the medium, so the mean energy loss is proportional to the density of the medium. The remaining dependence on the medium is weak because $Z/A \approx 0.5$ for all atoms except the very light and the very heavy elements, and because the ionisation energy I only enters the Bethe-Bloch formula logarithmically.

The mean excitation (ionisation) potential I is the main parameter in the Bethe-Bloch formula. It ranges from 13.5 eV in hydrogen to 1 keV in lead. The mean ionisation potential per electron depends on the atomic number of the atom. It is very difficult to calculate I so instead values of for several materials have been deduced from actual measurements of dE/dx, see Fig. 1.2. An approximate semi-empirical formula for I versus Z can be written as $I = 10Z$ eV for Z greater than 20. A slightly better approximation is given by

$$\frac{I[\text{eV}]}{Z} = \begin{cases} 12 + \frac{7}{Z} & \text{for } Z < 13, \\ 9.76 + 58.8Z^{-1.19} & \text{for } Z \geq 13. \end{cases} \tag{1.8}$$

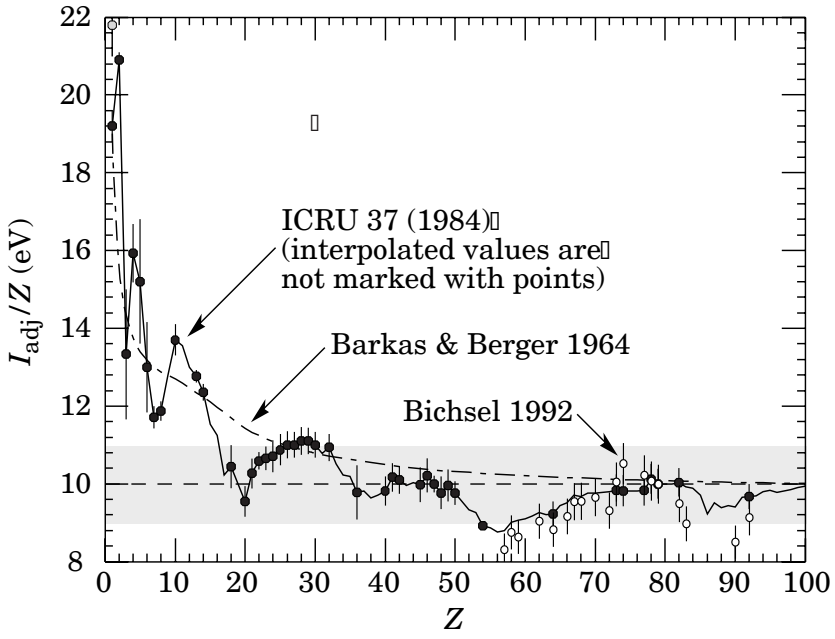

Figure 1.2: Mean excitation energies (divided by Z) as adopted by the ICRU. Those based on experimental measurements are shown by symbols with error bars. [PDG]

The expression in brackets in Eq. (1.7) varies slowly with particle energy. Thus, the general behaviour of dE/dx can be inferred from the behaviour of the multiplicative factor. For a given nonrelativistic particle, dE/dx therefore varies as $1/\beta^2$, or inversely with the particle energy. This behaviour can be heuristically explained by noting that because the charged particle spends a greater time in the vicinity of any given electron when its velocity is low, the impulse felt by the electron, and hence the energy transfer, is largest. Particles with the greatest charge will have the largest specific energy loss. High atomic number, high-density materials will result in the greatest linear stopping power.

Some example Beth-Block curves are shown in Fig. 1.3. The Bethe-Block formula can be considered as a function of velocity, or kinetic energy. At non-relativistic energies dE/dx is dominated by the overall $1/\beta^2$ factor and decreases with increasing velocity until a minium is reached. Particles at this point are minimum ionising. Broad minima occur at $\beta\gamma = 3.5$ to 3.0, as Z varies from 7 to 100. The minimum velocity is $\beta \approx 0.95$. The minimum value of dE/dx is almost the same for all particles of the same charge. The Z dependence of the minium value of dE/dx is shown in Fig. 1.4. Often in particle physics $\beta\gamma \approx 3$ so most particles are minimum ionising particles (mips). As the energy increases beyond this point, the factor $1/\beta^2$ becomes almost constant and dE/dx rises again due to the logarithmic

dependence of $\ln\gamma^2$. The rise part is referred to as the region of relativistic rise. The density effect (see below) causes the energy loss in the region of relativistic rise to only increase like $\ln\gamma$ instead of $\ln\gamma^2$, and causes the loss to become constant at very large γ. The constant ionisation loss at large γ is referred to as the Fermi plateau.

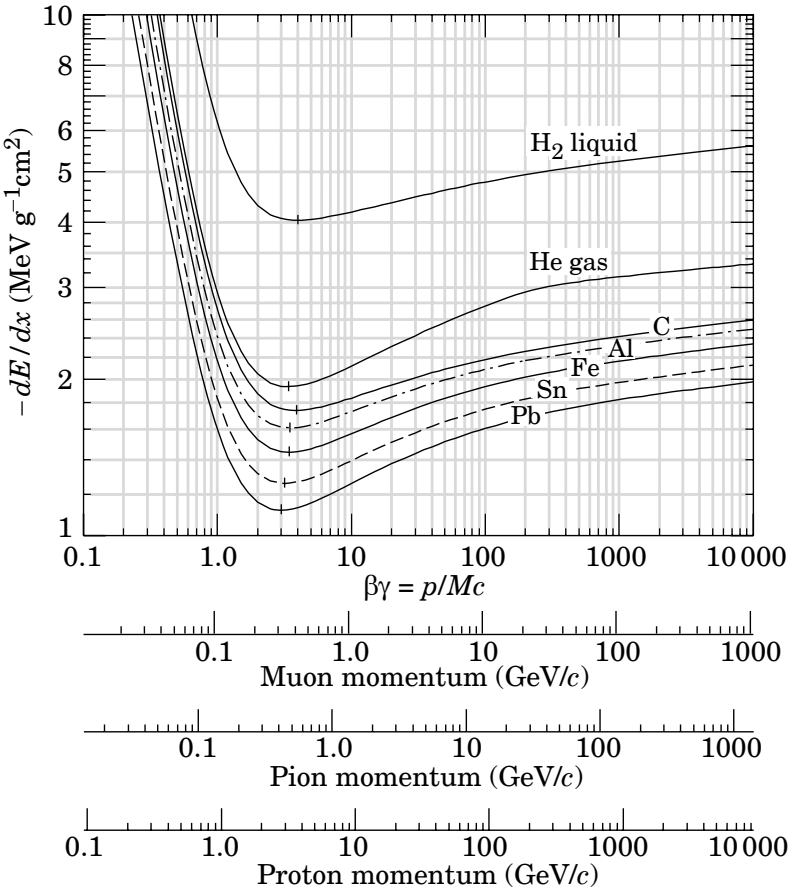

Figure 1.3: Mean energy loss rate for pions in liquid hydrogen, gaseous helium, carbon, aluminium, iron, tin, and lead. Radiative effects, relevant for pions, are not included. [PDG]

At energies below the minium ionising value, each particle exhibits a dE/dx curve which, in most cases, is distinct from the other particle types, see Fig. 1.5. This characteristic is often exploited in particle physics as a means for identifying particles in this energy range.

The derivation of the energy loss expression Eq. (1.7) makes use of a number of simplifying assumptions. At the low β extreme, atomic-shell corrections are necessary when the velocity of the incident particle becomes comparable to the velocity of the bound electrons. While at large γ, radiation, kinematic, and incident particle structure corrections may be necessary. In practice, two corrections are normally added to the Bethe-Block formula:

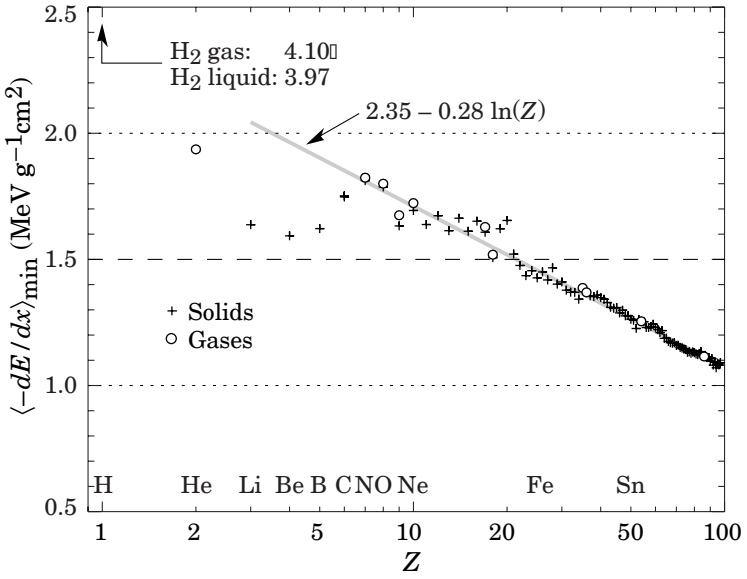

Figure 1.4: Stopping power at minimum ionisation for the chemical elements. The straight line is fitted for $Z > 6$. A simple functional dependence on Z is not to be expected, since $\langle -dE/dx \rangle$ also depends on other variables. [PDG]

1. a density effect correction δ (important at high energies) and

2. a shell correction C (important at low energies).

$$-\left\langle \frac{dE}{dx} \right\rangle = K \frac{Z}{A} \frac{z^2}{\beta^2} \left[\ln \frac{2m_e c^2 \beta^2 \gamma^2}{I} - \beta^2 - \frac{\delta(\gamma)}{2} - \frac{C}{Z} \right] . \tag{1.9}$$

The density effects arises from the fact that the electric field of the particle tends to polarise the atoms along its path. Because of this polarisation, electrons far from the path of the particle will be shielded from the full electric field intensity. Collisions with these outer lying electrons will therefore contribute less to the total energy loss than predicted by the Bethe-Block formula. The effect depends on the density of the material since the induced polarisation will be greater in condensed materials than in lighter substances such as gases, and hence the term density effect. Density corrections are needed for H_2.

The shell correction accounts for effects which arise when the velocity of the incident particle is comparable, or smaller, than the orbital velocity of the bound electrons. At such energies, the assumption that the electron is stationary with respect to the incident particle is no longer valid and the Bethe-Bloch formula breaks down.

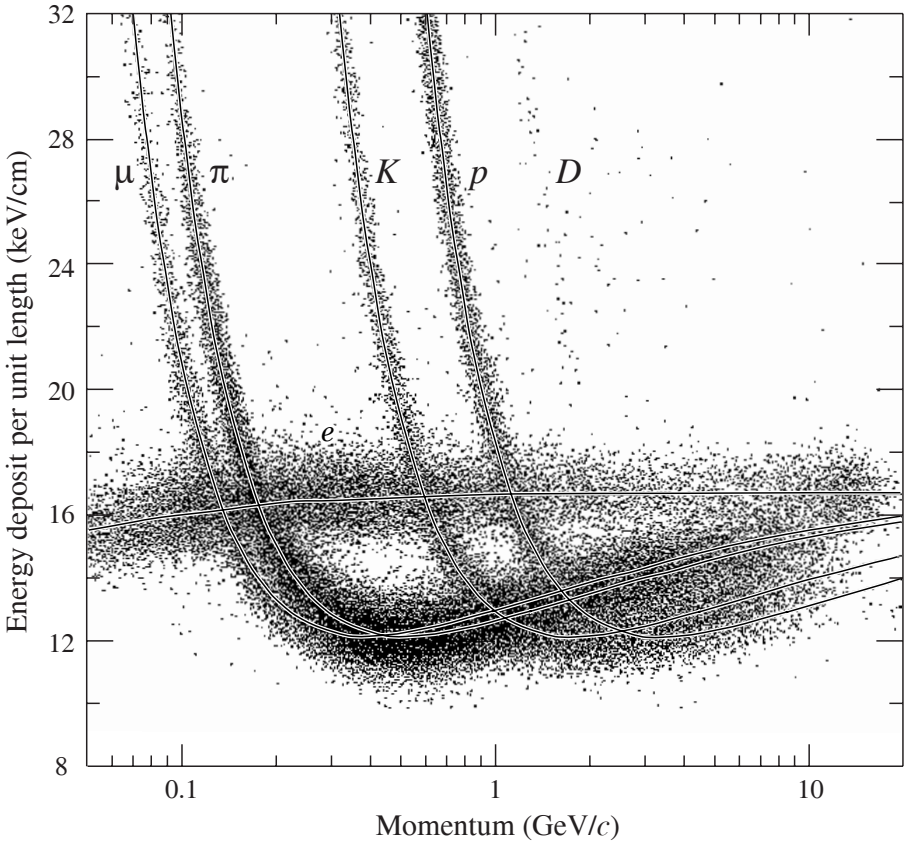

Figure 1.5: The PEP4/9-TPC energy deposit measurements (185 samples, 8.5 atm Ar-CH_4 80:20). The ionisation rate at the Fermi plateau (at high β is 1.4 times that for the minimum at low β. This ratio increases to 1.6 at atmospheric pressure. [PDG]

1.1.2 Fluctuations in Energy Loss

The amount of energy lost by a charged particle that has traversed a fixed thickness of absorber will vary due to the statistical nature of its interaction with individual atoms in the material. The values of dE/dx calculated in the preceding section are an averaged values. The mean of the energy-loss given by the Bethe-Bloch equation is ill-defined experimentally and is not useful for describing energy loss by single particles. (It finds its application in dosimetry, where only bulk deposit is of relevance.) It rises as $\ln \beta\gamma$ because $T_{\max}$ increases as $\beta^2\gamma^2$. The large single-collision energy transfers that increasingly extend the long tail are rare, making the mean of an experimental distribution consisting of a few hundred events subject to large fluctuations and sensitive to cuts as well as to background. Collisions with small energy transfers are more likely than those with large transfers. Thus, the most probable energy loss will be shifted to the lower half of the range of possible energy transfers. The result is that the energy loss distribution will be asymmetric with a tail on the high energy side. The most probable energy loss should be used, as shown in Fig. 1.6.

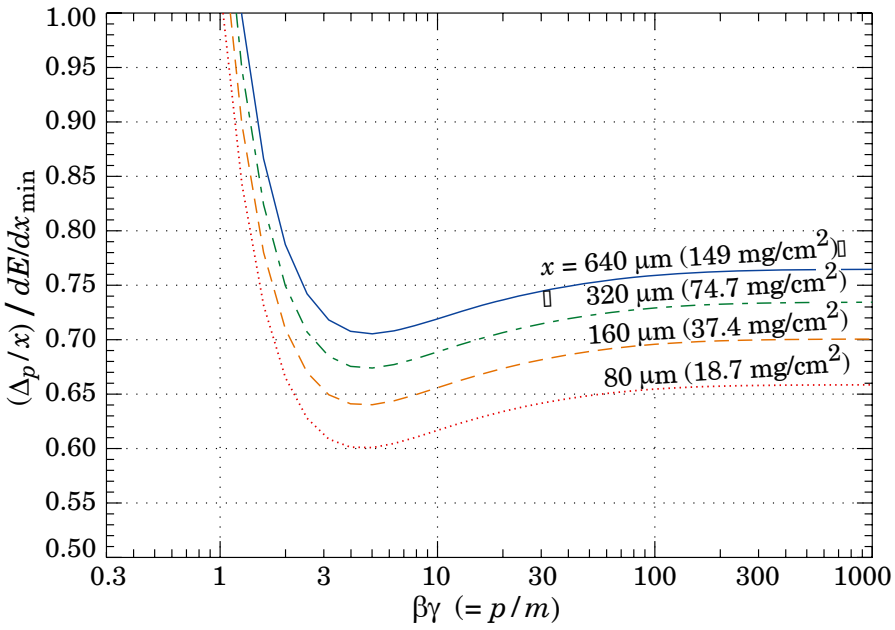

Figure 1.6: Most probable energy loss in silicon, scaled to the mean loss of a minimum ionising particle, 388 eV/μm (1.66 MeV g^{-1} cm^2).

For a detector of moderate thickness x, the energy loss probability distribution is adequately described by the highly-slewed Landau distribution. The most probable energy loss is

$$\Delta_p = \xi \left[\ln \frac{2mc^2\beta^2\gamma^2}{I} + \ln \frac{\xi}{I} + j - \beta^2 - \delta(\beta\gamma) \right] , \tag{1.10}$$

where $\xi = (K/2)\langle Z/A\rangle(x/\beta^2)$ MeV for a detector with a thickness x in g cm^{-2}, and $j = 0.200$. While dE/dx is independent of thickness, Δ_p/x scales as $a \ln x + b$. Folding in experimental also resolution displaces the peak. For very thick absorbers the distribution is less skewed but never approaches a Gaussian. While Δ_p/x may be calculated adequately, the distributions are significantly wider than the Landau width $w = 4\xi$. The width of the energy distribution is a measure of energy straggling, which varies with the distance along the particle track, see Fig. 1.7.

1.1.3 Range of Heavy Charged Particles

As a heavy charged particle passes though matter the interactions tend to cause small perturbations that reduce the particle's energy by small amounts and cause small changes in the particle's trajectory, but otherwise the particle is basically undisturbed. Thus, the number of heavy particles in monoenergetic a beam remains roughly constant until the velocities of

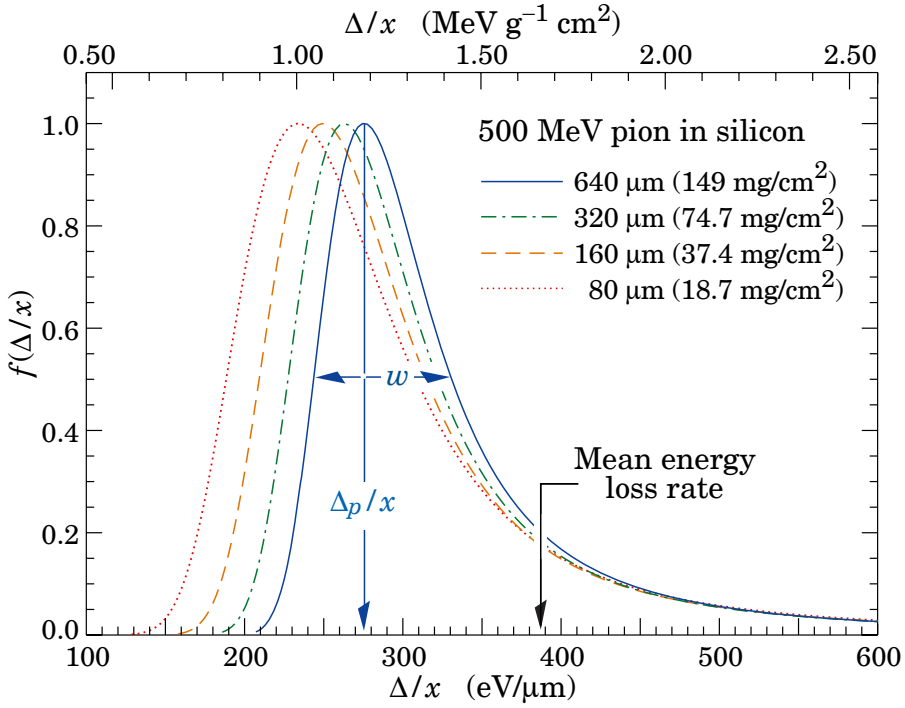

Figure 1.7: Straggling functions in silicon for 500 MeV pions, normalised to unity at the most probable value Δ_p/x. The width w is the full width at half maximum.

the particles have been reduced to a small values. Ultimately they will all be stopped after having crossed practically the same thickness of absorber, see Fig. 1.8.

The mean range R_m is defined as the absorber thickness that reduces the particle count to exactly one-half of its value in the absence of absorber. Another definition is the extrapolated range R_e, which is obtained by extrapolating the linear portion of the end of the transmission curve to zero. In practice, range is a useful concept only for low-energy hadrons ($R \lesssim \lambda_I$). Figure 1.9 shows the range of heavy charged particles in some absorbers.

From a theoretical point of view, we might calculate the mean range of a particle of a given energy by integrating the dE/dx formula. This is the continuous slow-down approximation (CSDA). This yields the approximate path length travelled. It ignores the effect of multiple Coulomb scattering, which causes the particle to follow a zigzag path through the absorber. The range defined as the straight-line thickness will generally be smaller than the total zigzag path length. As it turns out, the effect of multiple scattering is generally small for heavy charged particles so that the total path length is a relatively good approximation to the straight-line range.

If we assume that the energy loss is continuous, the distance must be a well defined number, the same for all identical particles with the same initial energy in the same type of material. This quantity is called the range of the particle, and depends on the type of

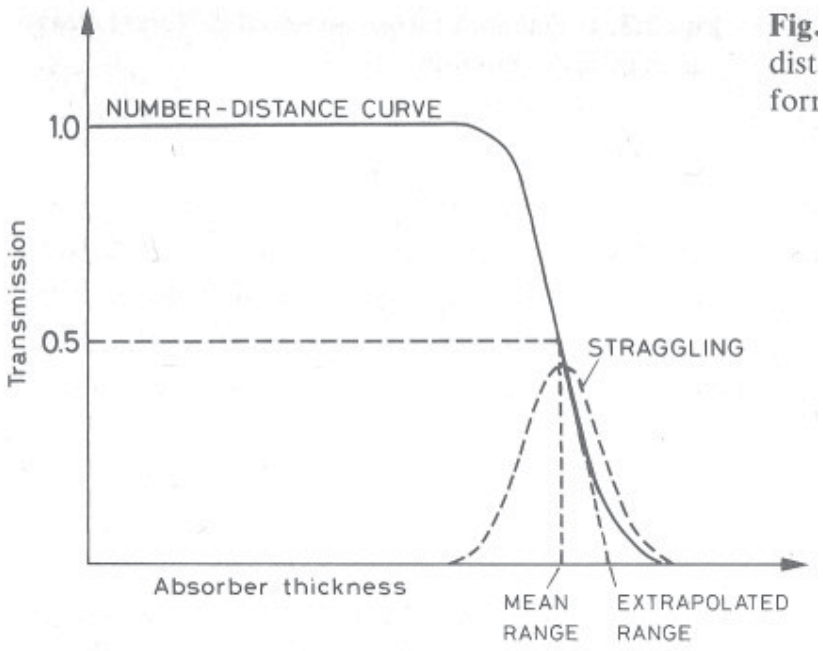

Figure 1.8: Number of particles versus penetration depth in an absorber. (transmission curve) The mean range R_m and extrapolated range R_e are indicated.

material, the particle type, and its energy. The energy loss is not in fact continuous, but statistical in nature. Two identical particles will show a statistical distribution of ranges cantered about some mean value. This phenomenon is known as range straggling. In first approximation this distribution is Gaussian. For heavy charged particles such as protons or alphas, the straggling amounts to a few percent of the mean range. The degree of straggling is evidenced by the sharpness of the cutoff at the end of the average transmission curve. Differentiating this curve leads to a peak whose width is often taken as a quantitative measure of the importance of range straggling for the particle and absorber used in the measurement.

As a heavy particle slows down in matter, its rate of energy loss will change as its kinetic energy changes. Because of the factor β^{-2}, most of the ionisation loss occurs near the end of the path where the speed is smallest. More energy per unit length will be deposited towards the end of its path rather than at the beginning. At the very end it begins to pick up electrons and the dE/dx drops. The curve has a pronounced peak close to the end point before falling rapidly to zero at the end of the particle's path length. A plot of the specific energy loss along the track of a charged particle is known as a Bragg curve, Fig. 1.10. The peak is called the Bragg peak.

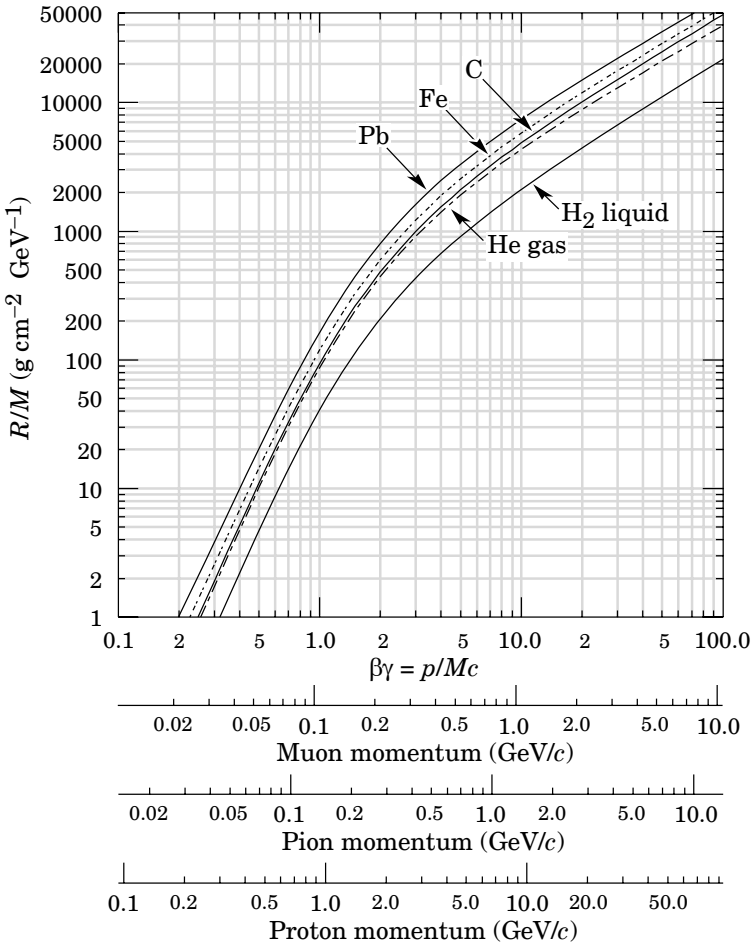

Figure 1.9: Range of heavy charged particles in liquid (bubble chamber) hydrogen, helium gas, carbon, iron, and lead.

1.2 Energy Loss of Electrons and Positrons

At low energies electrons and positrons primarily lose energy by ionisation. Excitation and ionisation are not the only causes of energy loss. Because of their small mass, they also have significant losses due to the production of radiation, bremsstrahlung, arising from scattering in the electric field of a nucleus. While ionisation loss rates rise logarithmically with energy, bremsstrahlung losses rise nearly linearly (fractional loss is nearly independent of energy), and dominates above a few tens of MeV in most materials, see Fig. 1.11 Ionisation dominates over radiation for $E \ll 2mc^2$. Other significant sources of energy loss for low energy electrons are elastic scattering and positron annihilation. At large γ other contributing processes include Cherenkov radiation, transition radiation, and pair production, which will not be discussed here. For high energy electrons, the bremsstrahlung and pair production precesses

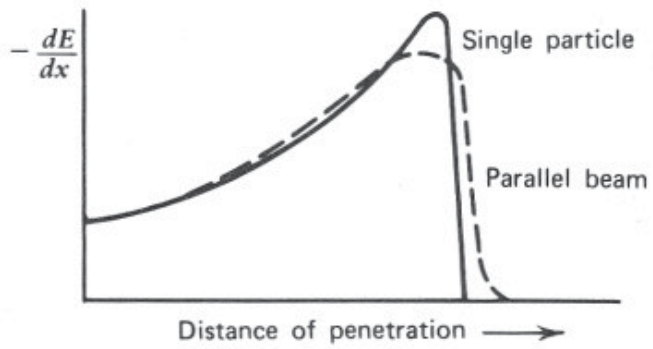

Figure 1.10: The specific energy loss along an alpha track.

lead to the production of electromagnetic showers.

The total energy loss of electrons and positrons is composed of two parts (collision and radiative losses):

$$\left(\frac{dE}{dx}\right)_{\text{tot}} = \left(\frac{dE}{dx}\right)_{\text{col}} + \left(\frac{dE}{dx}\right)_{\text{rad}} . \tag{1.11}$$

1.2.1 Collision Loss

The energy loss of electrons by ionisation may be treated in a manner similar that used for heavy ions, but there are several important differences. As a first approximation one can consider corresponding expression for the energy loss of the singly charged, heavy particles travelling at relativistic velocities ($\beta \approx 1$)

$$-\left\langle \frac{dE}{dx} \right\rangle = K\frac{Z}{A}\left(\ln\frac{2mc^2}{I} + 2\ln\gamma - 1\right) . \tag{1.12}$$

Ionisation loss by electrons and positrons differs from loss by heavy particles because of the kinematics (reduced mass of the electron), spin, and the identity of the incident electron with the electrons which it ionises. The Bethe-Bloch formula must be modified for two reasons:

1. The small electron mass. The assumption that the incident particle remains undeflected during the collision process is therefore invalid.

2. For electrons, the collisions are between identical particles, so that the calculation must take into account their indistinguishability.

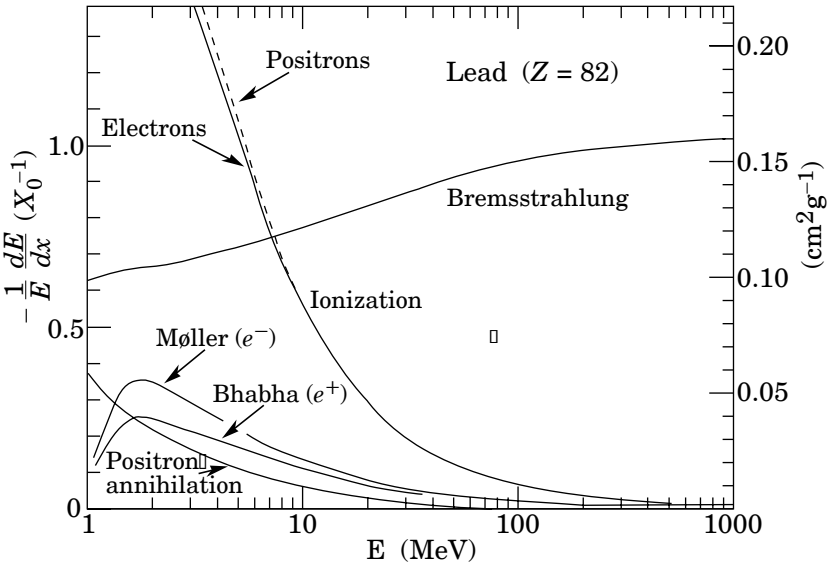

Figure 1.11: Fractional energy loss per radiation length in lead as a function of electron or positron energy.

These considerations change a number of terms in the formula, in particular, the maximum allowed energy transfered.

For electrons and positrons, the maximum allowable energy transfer becomes $W_{\max} = T_c/2$, where T_c is the kinetic energy of the incident electron or proton. The Bethe-Bloch formula for electrons and positrons is

$$-\left\langle \frac{dE}{dx} \right\rangle = \frac{K}{2}\frac{Z}{A}\frac{1}{\beta^2}\left[\ln\frac{\tau^2(\tau+2)}{2(I/m_ec^2)^2} + F(\tau) - \delta - 2\frac{C}{Z}\right], \tag{1.13}$$

where τ is the kinetic energy of the particle in units of m_ec^2. $F(\tau)$ is a function which is different for electrons and positrons. The energy loss for positrons differs slightly since the Bhabha differential cross section must be used in place of the Moller cross section.

Comparison of the two equations shows that to first order all singly charged particles with $\beta \sim 1$ lose energy by collisions at approximately the same rate. The second terms indicate that the rate of relativistic rise for electrons will be slightly smaller than for heavier particles.

1.2.2 Bremsstrahlung Radiation Loss

The dominant energy loss mechanism for high energy electrons is the production of electromagnetic radiation. This is usually referred to as synchrotron radiation for circular acceleration and bremsstrahlung for motion through matter. As a practical matter, electrons and positrons are the only particles in which radiation contributes substantially to the en-

ergy loss of the particle – at least at the current energies of particle physics today. The Bremsstrahlung emission probability varies as the inverse square of the particle mass, i.e., $\sigma \propto r_e^2 = (e^2/mc^2)^2$. Radiation loss by muons ($m = 106$ MeV), the next lightest particle, is thus some 40 000 times smaller than that for electrons.

The energy loss due to bremsstrahlung is given by

$$-\left\langle \frac{dE}{dx} \right\rangle_{\text{brem}} \equiv \frac{E}{X_0}\,, \tag{1.14}$$

where X_0 is the radiation length given by

$$X_0^{-1} = \begin{cases} 4\alpha N_A r_e^2 \frac{Z(Z+1)}{A} \left[\ln \frac{2E_0}{m_e c^2} - \frac{1}{3} - f(Z)\right] & \text{for } m_e c^2 \ll E_0 \ll m_e c^2/(\alpha Z^{1/3}), \\ 4\alpha N_A r_e^2 \frac{Z(Z+1)}{A} \left[\ln \frac{183}{Z^{1/3}} + \frac{1}{18} - f(Z)\right] & \text{for } E_0 \gg m_e c^2/(\alpha Z^{1/3}), \end{cases} \tag{1.15}$$

where $f(Z)$ is a small correction to the Born approximation which takes into account the Coulomb interaction of the emitted electron in the electric field of the nucleus. The first case is the approximation of no screening and the second case for complete screening. The mean energy loss from radiation in the field of just the nucleus is as above but $Z(Z+1)$ is replaced by Z^2. The mean energy loss from radiation in the field of just the the electrons is as above but $Z(Z+1)$ is replaced by Z. Thus $Z(Z+1)$ approximately accounts for both contributions.

X_0 is, in general, a function of electron energy and the nature of the absorber material. However, for electrons and photon energies above 1 GeV, X_0 is almost energy-independent. This expression is approximate and valid for $E \gg mc^2/(\alpha Z^{1/3})$ (relativistic electrons). This formula is valid under different hypothesis and differs only logarithmically in the energy. To better than 20% for about $Z > 13$,

$$X_0 \ [\text{g/cm}^2] \approx 180 \frac{A}{Z^2}\,. \tag{1.16}$$

The radiation length represents a characteristic amount of matter traversed. Integration of Eq. (1.14) gives

$$E = E_0 e^{-x/X_0}\,, \tag{1.17}$$

where E_0 is the initial energy. It follows that the radiation length is the mean distance over which a high-energy electron loses all but $1/e$ of its energy by bremsstrahlung. If x is expresses in units of X_0, then

$$-\frac{dE}{dt} \approx E\,, \tag{1.18}$$

where t is the distance in radiation lengths. Thus, the radiation energy loss when expressed in terms of radiation length is roughly independent of the material type.

The ratio of bremsstrahlung to ionisation energy loss is

$$\left\langle \frac{dE}{dx} \right\rangle_{\text{brem}} \Big/ \left\langle \frac{dE}{dx} \right\rangle_{\text{ion}} \equiv R \approx \frac{ZE}{1600mc^2} = \frac{ZE}{800}\,, \tag{1.19}$$

where E is in MeV. For

$$R \approx 1 \Rightarrow E \equiv E_c \approx \frac{800}{Z}\ \text{MeV}\,, \tag{1.20}$$

which for lead ($Z = 96$) is $E_c = 9.8$ MeV. The numerator is sometimes given as 600 or 700. The values are found to be different for solids and liquids, or gases. The denominator is sometimes given an offset of +1.2 or +0.9, again different for solids and liquids, or gases. Ionisation dominates at low energies and bremsstrahlung at high energies. Radiation losses are much smaller than ionisation losses for all particles other than electrons and positrons at all but the highest energies.

1.2.3 Range of Electrons

Because of the electron's greater susceptibility to multiple scattering by nuclei, the range of electrons is generally very different from the calculated path length obtained from an integration of the dE/dx formula. In addition, the energy loss by electrons fluctuates much more than for heavy particles. This is due to the much greater energy transfer per collision allowed for electrons and to the emission of bremsstrahlung. In both cases, it is possible for a few single collisions (or photons) to absorb the major part of the electron's energy. Thus, electrons of the same energy are not all stopped by the same thickness of material. This results in greater range straggling, and the concept of range has a limited validity.

1.2.4 Other Electromagnetic Effects

We will not discuss elastic scattering or multiple scattering. Although Rutherford scattering is also possible, such encounters occur only rarely and they are not normally significant in the response of radiation detectors.

Pair Production

Another process by which fast moving charged particles can lose energy is through direct pair production. The electromagnetic field of the charged particle may be considered as a flux of virtual photons. In the Coulomb field of the nucleus, or an electron, the virtual photons can decay into an electron and positron, just as real photons do in the process of pair production.

Positron Annihilation

The ultimate fate of most positrons in matter is annihilation with an electron into photons: $e^+e^- \rightarrow \gamma\gamma$. Annihilation into a single photon is possible if the electron is bound to a nucleus, but the cross section for this process is at most 20% of that for two photons.

1.3 Energy Loss of Photons

The behaviour of photons in matter is dramatically different from that of charged particles. In particular, the photon's lack of an electric charge makes impossible the many inelastic collisions with atomic electrons so characteristic of charged particles. For photons, on the other hand, the absorption is exponential.

The main interactions of photons in matter are:

1. photoelectric effect,
2. scattering on free electrons (Thomson, Rayleigh, and Compton scattering), and
3. pair creation.

Each process is complex and accompanied by secondary effects. The three processes have different relative importance in different spectral regions, depending on the atomic number of the absorber.

At low energies, the interaction is dominated by the photoelectric effect, while at high energies it is dominate by pair production. The Compton effect plays an important role at intermediate energies. Two other effect are coherent (Rayleigh) scattering and photonuclear absorption. Rayleigh scattering is a process in which photons scatter from the atomic electrons without excitation or ionisation of the atom. Photonuclear absorption is actually a nuclear interaction where the photon is absorbed by the nucleus. It is most important in the region of the giant resonance and is frequently accompanied by the emission of a neutron.

These reactions explain the two principle qualitative features of photons:

1. photons are many times more penetrating in matter than charged particles, and
2. a beam of photons is not degraded in energy as it passes through a thickness of matter, only attenuated in intensity.

The first feature is due to the much smaller cross section of the three processes relative to the inelastic electron collision cross section. The second characteristic is due to the fact that the three processes above remove the photon from the beam entirely, either by absorption or scattering.

In general, there is a large probability that an interacting photon will be removed from the beam. Consider a collimated, monoenergetic beam of N photons. The number removed from the beam while crossing a thickness dx of material is

$$dN = -\mu N dx\,, \tag{1.21}$$

where the constant of proportionality μ is known as the linear attenuation coefficient, and is related to the probability that a photon will be scattered or absorbed in the material.

In a homogeneous medium, the intensity of a beam of collimated, monoenergetic photons decreases exponentially

$$I(x) = I_0 \exp(-\mu x)\,, \tag{1.22}$$

where μ is the linear attenuation coefficient. The coefficient μ is often divided by the density to obtain the mass attenuation coefficient μ/ρ, which has the units cm^2/g. The mass attenuation coefficient is related to the total photon interaction cross section σ_{tot} by

$$\frac{\mu}{\rho} = \frac{N_A}{A}\sigma_{\mathrm{tot}} \approx \frac{N_A}{A}\left[\sigma_{\mathrm{photoelectric}} + Z\sigma_{\mathrm{Compton}} + \sigma_{\mathrm{pair}}\right]\,, \tag{1.23}$$

where A is the atomic weight of the material. We have multiplied the Compton cross-section by Z to take into account the Z electrons per atom. Figure. 1.12 shows the energy dependence of the different contributions to the absorption coefficient.

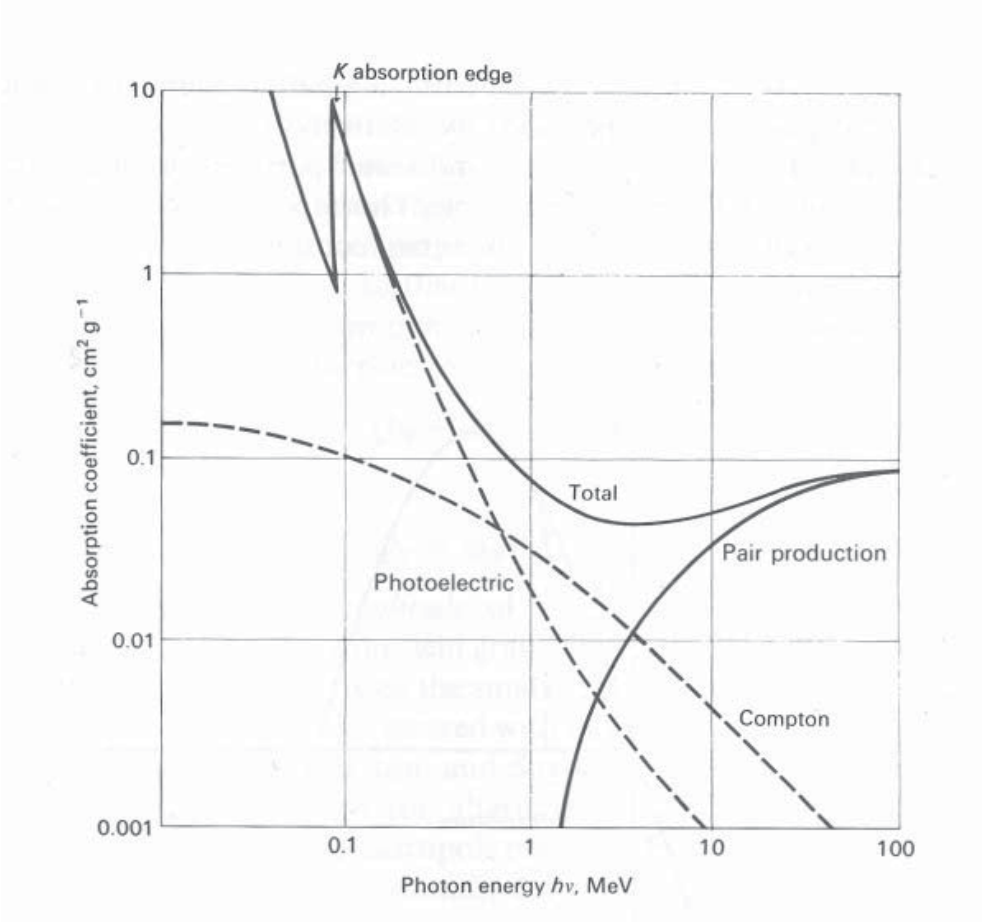

Figure 1.12: Absorption coefficient per g cm^{-2} of lead for gamma rays as a function of energy.

1.3.1 Photoelectric Effect

The photoelectric effect can be considered to be an interaction between the photon and the atom as a whole. Incident photons whose energy exceeds the binding energy of an electron in the atom may be absorbed, and an atomic electron ejected with kinetic energy.

There are sharp discontinuities in the photoelectric spectrum corresponding to the binding energies of the atomic shells, the most prominent of which is due to the innermost, or K-shell. The energies are given approximately by Moseley's law:

$$E = Rhc\frac{(Z-\sigma)^2}{n^2}\,, \tag{1.24}$$

where $Rhc = 13.605$ eV, σ the screening constant, and n the principle quantum number of the different electronic orbits. The screening constant has the approximate value 3 for the K-shell and 5 for the L-shell.

The vacancy created by the ejection of an electron from the inner shells is filled by outer electrons falling into it, and this process may be accompanied by the emission of fluorescent radiation. Alternatively it is possible that no fluorescent radiation is emitted but that an electron from the outer shell is ejected. These and similar processes, are call Auger processes.

1.3.2 Compton Scattering

This is the scattering of photons on free electrons. In matter, the electrons are bound. However, if the photon energy is high with respect to the binding energy, the binding energy can be ignored, and the electrons can be considered as essentially free.

Thomson and Rayleigh Scattering

Related to Compton scattering are the classical processes of Thomson and Rayleigh scattering. Thomson scattering is the scattering of photons by free electrons in the classical limit. Rayleigh scattering is the scattering of photons by atoms as a whole. In this process, all the electrons in the atom participate in a coherent manner. For this reason, it is also called coherent scattering. In both precesses, the scattering is characterised by the fact that no energy is transferred to the medium. The atoms are neither excited nor ionised, and only the direction of the photon is changed.

1.3.3 Pair Production

The intense electric field near the nucleus can cause the photon to decay into an electron and a positron. This is the process of pair production. In order to conserve momentum, this can only occur in the presence of a third body, usually a nucleus. The nucleus must be there to satisfy conservation of momentum, but it acquires very little recoil energy. For the case of pair production in the electric field of an electron, the threshold energy is $2mc^2$, and the recoil electron acquires significant kinetic energy.

To obtain the total pair production cross section, a numerical integration must generally be performed. In the case of no screening with $h\nu \gg 137 m_e c^2 Z^{-1/3}$, an analytic integration is possible yielding

$$\sigma_{\text{pair}} = 4\alpha r_e^2 Z^2 \left\{ \frac{7}{9} \left[\ln \frac{183}{Z^{1/3}} - f(Z) \right] - \frac{1}{54} \right\} . \tag{1.25}$$

As for bremsstrahlung, pair production may also occur in the field of an atomic electron. Not surprisingly, a similar result is obtained for the cross section, but smaller by a about a factor of Z. To approximately account for this interaction, then, one need only replace Z^2 by $Z(Z+1)$ in the above formulae.

From the total cross section, it is interesting to calculate the mean free path X_p of a photon from pair production

$$\frac{1}{X_p} = N\sigma_{\text{pair}} \approx \frac{7}{9} 4\alpha r_e^2 N Z(Z+1) \left[\ln \frac{183}{Z^{1/3}} - f(Z) \right] , \tag{1.26}$$

where N is the density of atoms and we have ignored the small constant term. This may be recognised as begin very similar to the radiation length, and, in fact, comparison shows

$$X_p = \frac{9}{7} X_0 . \tag{1.27}$$

Radiation length is characteristic amount of mater traversed. It is 7/9 of the mean free path for pair production by a high-energy photon.

1.4 Electron and Photon Showers

To detect a particle it must undergo an interaction in a detector. The interaction of a high-energy photon or electron leads to a cascade of electrons and photons. Bremsstrahlung and pair production combine to produce showers. A high energy photon in matter converts into an electron and positron pair which then emits energetic bremsstrahlung photons. These in turn will convert into further electron-positron pairs, and so on. The result is a cascade or shower of photons, electrons, and positrons. This continues until the energy of the pair-produced electrons and positrons drops below the critical energy. At this point, the electron-positron pairs will preferentially lose their energy via atomic collisions rather than bremsstrahlung emission, thus halting the cascade.

The development of the cascade is a statistical precess. In describing shower behaviour it is convenient to introduce the scaled variables

$$t = \frac{x}{X_0} \quad \text{and} \quad y = \frac{E}{E_c} , \tag{1.28}$$

so that distance is measured in units of radiation length and energy in units of critical energy. By using the notion of radiation length we may construct a simple model to describe the mean number of particles produced and their mean energies as a function of penetration depth

in the converting material. Starting with a photon of energy E_0, after one radiation length X_0 on average the photon converts into an electron-positron pair with average energy $E_0/2$. After two radiation lengths the electron and positron will then each emit a bremsstrahlung photon with approximately half the energy of the charge particle. At this point there are four particles present: two photons and an electron-positron pair, each with energy $E_0/4$. At the end of three radiation lengths the bremsstrahlung photons will have converted into two more electron-positron pairs, while the original pair will have emitted another set of bremsstrahlung photons. The number of particles present is thus eight and their energy is $E_0/8$. Continuing in this manner, at the end of t radiation lengths, the total number of particles (i.e., photons, electrons, and positrons) will be

$$N \approx 2^t = e^{t \ln 2} \tag{1.29}$$

each with an average energy of

$$E(t) \approx \frac{E_0}{2^t} \,. \tag{1.30}$$

This simple model is sometime referred to as the Heitler model. The same result would also be obtained had we started with an electron rather than a photon. In this case, the simple shower is shown in Fig. 1.13.

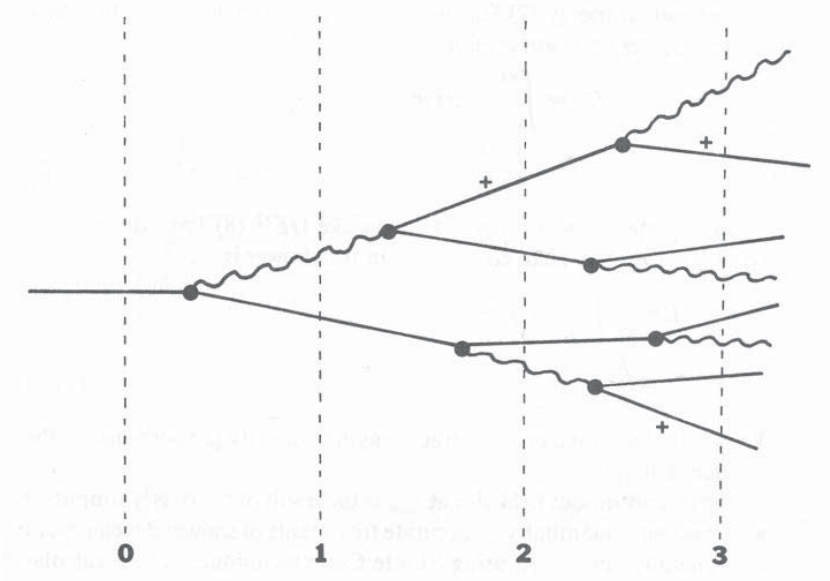

Figure 1.13: Simple model for the development of an electromagnetic shower. Solid lines (with +) indicate electrons (positrons) and wavy lines indicate photons. The numbers at the bottom show the distance measured in radiation lengths. [Fernow]

The cascade stops approximately when the particles approach the critical energy, i.e., if $E_0/2^t = E_c$. That is

$$E(t_{\max}) = \frac{E_0}{2^{t_{\max}}} = E_c \,. \tag{1.31}$$

The number of generations up to the maximum is

$$t_{\max} = \frac{\ln\left(E_0/E_c\right)}{\ln 2} \,. \tag{1.32}$$

The number of particles at the maximum is

$$N_{\max} \approx \frac{E_0}{E_c} \,. \tag{1.33}$$

The maximum number of particles is proportional to the initial particle energy. The total integral track length of charged particles (in radiation lengths) in the whole shower will be

$$L \approx \frac{E_0}{E_c} \,. \tag{1.34}$$

The discontinuous behaviour at $t_{\max}$ is the result of the overly simplified assumptions. This simple model only gives a rough qualitative picture of the shower. In reality, the number of particles in an electron-photon cascade rises exponentially to a broad maximum after which it declines gradually, see Fig. 1.14. In general, a precise calculation cannot be made analytically and recourse must be made to such techniques as Monte Carlo simulations.

Empirically, the maximum number of electrons occur at the depth

$$t_{\max} = 3.9 + \ln E_0 \,, \tag{1.35}$$

where $t_{\max}$ is measured in radiation lengths and E_0 in GeV. The number of electrons at the maximum is given by

$$N_{\max} = 8.45 E_0^{0.935} \,. \tag{1.36}$$

The total path length of electrons in the shower is

$$L(E_0) = 60.2 E_0 \,. \tag{1.37}$$

The energy dependence of the last three equations are in qualitative agreement with the simple model.

The mean longitudinal profile of the energy deposition in an electromagnetic cascade is reasonably well described by a gamma distribution:

$$\frac{dE}{dt} = E_0 b \frac{(bt)^{a-1} e^{-bt}}{\Gamma(a)} \,, \tag{1.38}$$

where a and b are fit parameters, and

$$t_{\max} = \frac{a-1}{b} = 1.0 \times (\ln y + C_j), \quad j = e, \gamma, \tag{1.39}$$

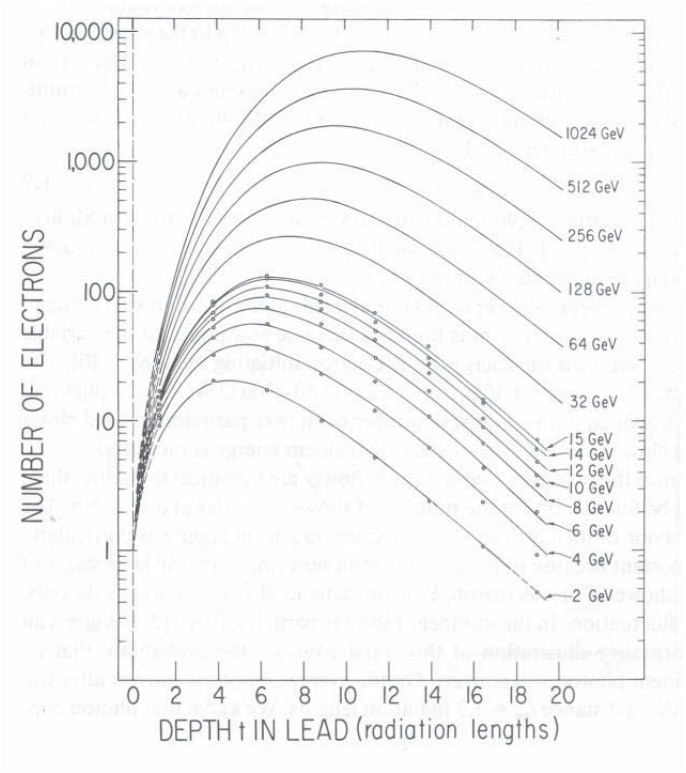

Figure 1.14: Shower profiles in lead. The number of electrons should be multiplied by a normalisation factor of 0.79 [Fernow]

where $C_e = -0.5$ for electron-induced cascades and $C_\gamma = +0.5$ for photon-induced cascades. One can fit for both a and b, or assume $b \approx 0.5$ and fit for a. This empirical function fails badly for the first two radiation lengths. Because fluctuations are important, the Gamma distribution should be used only in applications where average behaviour is adequate, see Fig. 1.15.

As shown in Fig. 1.16, the longitudinal development of electromagnetic showers in different materials is found to scale if distances are measured in radiation lengths.

Since at high energies the angles of emission of the electrons and photons are small, the shower will develop primarily in the forward direction. It is then customary to treat separately the longitudinal and transverse development.

The transverse dimension of a shower is determined by the multiple scattering of low energy electrons. The distributions are characterised by a narrow cone, and broaden as the shower develops. A useful unit for transverse shower distributions is the Moliere radius

$$R_M = 21 \frac{X_0}{E_c} \text{ MeV}\,. \tag{1.40}$$

The distribution of shower energy in transverse (radial) bins scales in R_M, is independent

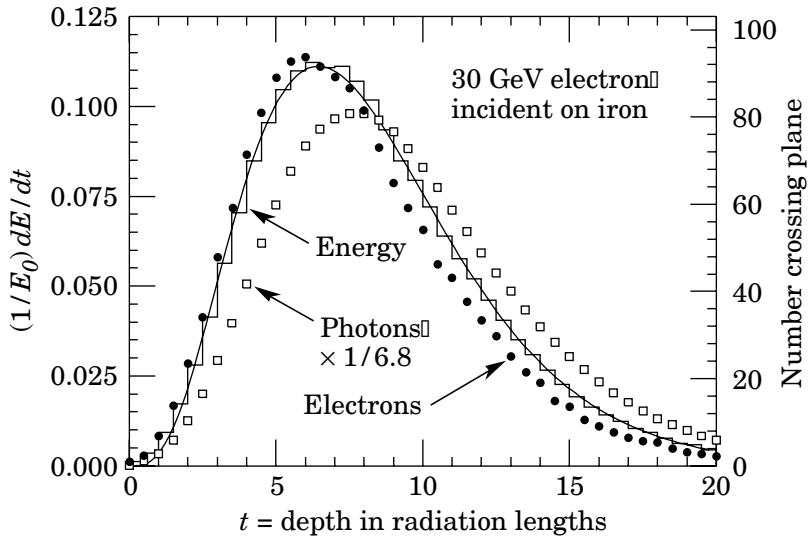

Figure 1.15: An EGS4 simulation of a 30 GeV electron induced cascade in iron. The histogram shows fractional energy deposition per radiation length, and the curve is a gamma-function fit to the distribution. Circles indicate the number of electrons with total energy greater than 1.5 MeV crossing planes at $X_0/2$ intervals (scale on right) and the squares the number of photons with $E \geq 1.5$ MeV crossing the planes (scaled down to the same area as the electron distribution). [PDG]

of the material used. On the average, only 10% of the energy lies outside the cylinder with radius R_M, which is about $3X_0$ for Pb. About 99% of the energy is contained inside the radius of $3.5R_M$. Roughly 95% of the shower is contained laterally in a cylinder with radius $2R_M$.

Figure 1.14 also shows the shower radius at each depth that contains 90% of the shower particles. Up to the shower maximum the shower is contained in a cylinder with radius less than one radiation length. Beyond that point the electrons are increasingly affected by multiple scattering, and the lateral size scales in the Moliere radius, as

$$R_M \approx 7\frac{A}{Z}\ \mathrm{g/cm^2}\,. \tag{1.41}$$

The number of shower tracks found inside a ring of radius r at the depth of the shower maximum is found to increase as a power of the variable rE_0. The result is independent of E_0 over a large range. This implies that a cylinder containing a fixed number of shower particles is found closer and closer to the shower axis as the incident energy increases.

Let us now consider the oversimplified shower model. The conservation of momentum gives to the whole shower an axis in the direction of the momentum of the first electron. The shower spreads laterally much less than it propagates longitudinally. Thus the following

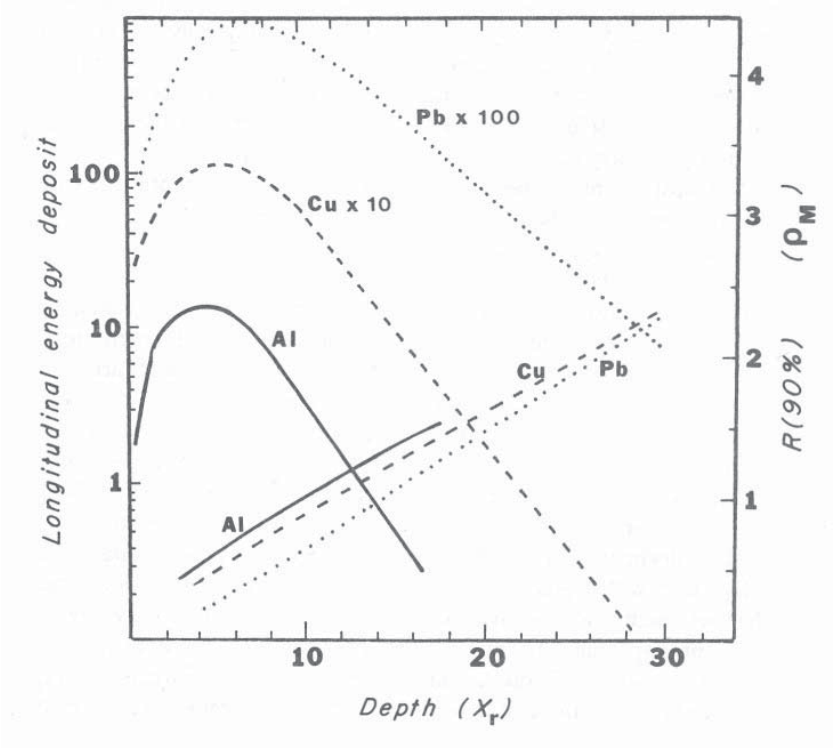

Figure 1.16: Longitudinal development of electromagnetic showers in different materials. Right scale shows radii for 90% shower containment. [Fernow]

discussion will be limited to the shower propagation in the direction of the initial particle. An electron of energy E gives rise in one radiation length to about three gamma rays, which in turn, give rise in a mean free path to about three pairs. The number of particles in the shower, N, start to grow exponentially with the progress of the shower:

$$N(x) = e^{\gamma x}\,, \tag{1.42}$$

where γ is such that for $x_1 = X_0 + X_p$, $N = e^{\gamma x_1} = 6$, but

$$X_0 + X_p = \frac{16}{7} X_0 \tag{1.43}$$

and hence

$$\gamma = \frac{\ln 6}{(16/7)X_0} = \frac{0.78}{X_0}\,. \tag{1.44}$$

In an actual shower, electrons, positrons, and photons are simultaneously present. Furthermore, the number of photons, especially of low energy, ends by being approximately twice as large as the number of particles. The number of particles in the shower increases until energy starts to dissipate, primarily by ionisation and the Compton effect rather than

radiation and pair production. At this point the particles have reached the energy E_c, and if we assume that the average energy of electrons, positrons, and photons is the same, namely E_c, their number is $E_0/(3E_c)$. This occurs at a distance

$$X_c = \frac{X_0}{0.78} \ln \frac{E_0}{3E_c} \tag{1.45}$$

from the origin, and

$$N_{\max} = \frac{E_0}{3E_c} = e^{0.78X_c/X_0} \,. \tag{1.46}$$

This estimate neglects energy losses by ionisation, the energy going into the rest mass of the pairs, and other important factors that depress $N_{\max}$ to a value near $E_0/(6E_c)$. More detailed expressions for high energy and low Z are

$$N_{\max} = 0.31 \frac{E_0}{E_c} \left(\ln \frac{E_0}{E_c} - 0.37 \right)^{-1/2} \tag{1.47}$$

and

$$X_c = 1.01 X_0 \left(\ln \frac{E_0}{E_c} - 1 \right) . \tag{1.48}$$

The total integral path length S of all electrons and positrons in the shower is approximately

$$S = \frac{2}{3} X_0 \sum_{\nu=1}^{n} 2^\nu + s_0 \frac{2}{3} N_{\max} = \left(\frac{4}{3} X_0 + \frac{2}{3} s_0 \right) \frac{E_0}{E_c} \,, \tag{1.49}$$

where s_0 is the path length of electrons below the critical energy. The path length S is proportional to the total energy E_0 if electrons and positrons can be detected until they come to rest. In practical detectors, there is a minimum kinetic energy required for detection (cut-off energy E_k). Thus the visible path becomes

$$S = F(z) X_0 \frac{E_0}{E_c} \,, \tag{1.50}$$

where $F(x) \approx e^z[1 + z \ln(z/1.526)]$ and $z = 4.58 Z E_k/(A E_c)$.

Including the effect of the cut-off energy into Monte Carlo calculations gives the following properties of electron-photon showers.

1. The number of particles at maximum $N_{\max}$ is proportional to the primary energy E_0.

2. The total track length of electrons and positrons S is proportional to E_0.

3. The depth at which the maximum occurs $X_{\max}$ increases logarithmically: $X_{\max}/X_0 = \ln(E_0/E_c)t$, where $t = 1.1$ for electrons and $t = 0.3$ for photons.

1.5 Interactions of Neutrons

Like the photon, the neutron lacks an electric charge, so that it is not subject to Coulomb interactions with the electrons and nuclei in matter. Instead, its principle means of interaction is through the strong force with the nuclei. Neutrons must come within the size of the nucleus before anything can happen, and since normal matter is mainly empty space, it is not surprising that the neutron is observed to be a very penetrating particle.

When the neutron does interact it can undergo a variety of nuclear processes:

1. Elastic scattering from nuclei,
2. Ineleasitc scattering,
3. Radiative neutron capture,
4. Fission,
5. High energy hadron shower production,
6. Other nuclear reactions.

Because of the strong energy dependence of neutron interactions, it has become customary to classify neutrons according to their energy:

1. high energy neutrons (above 100 MeV),
2. fast neutrons (few tens MeV to few hundred keV),
3. epthermal (100 keV to 0.1 eV, where nuclear resonance reactions occur),
4. thermal or slow (energies compared to thermal agitation energies at room temperature),
5. cold or ultra-cold (energies of milli-eV or micro-eV).

1.5.1 Hadronic Showers

The average longitudinal distribution rises to a smooth peak about one nuclear interaction length (λ_I) into the calorimeter. It then falls somewhat faster than exponentially. Proton-induced cascades are somewhat shorter and broader than pion-induced cascades. The longitudinal development of hadronic showers scales with the nuclear absorption length, but the lateral shower development does not.

The transverse energy deposit is characterised by a central core dominated by EM cascades, where the neutral meson parents are themselves produced at a variety of angles. There is a wide "skirt" produced by wide-angle hadronic interactions. The energy deposited in an annulus is adequately described by an exponential core and a Gaussian halo.

The parameter corresponding to the radiation length X_0 in electromagnetic showers is the nuclear absorption length:

$$\lambda_I = [(\text{nuclei/unit volume}) \cdot \sigma_I]^{-1} = \frac{A}{N_A \rho \sigma_I}\,, \tag{1.51}$$

where σ_I the inelastic nucleon cross-section (absorption cross-section). σ_I and hence λ_I vary with energy for energies in the region of the nucleon resonances, but above about 2 GeV, λ_I is almost energy-independent. A rough approximation is given by

$$\lambda_I \approx 35 A^{1/3} \text{ g cm}^{-2}\,. \tag{1.52}$$

The lateral shower size is such that about 95% of the energy is deposited within a cylinder of radius λ_I.

The longitudinal development of hadronic showers scales with the nuclear absorption (or interaction) length. The lateral shower development does not scale with λ_I. The physical process responsible for hadronic showers is different from electromagnetic showers. About half of the incident hadron energy is passed on to additional fast secondaries. The remainder is consumed in multiparticle production of slow pions and in other processes. The secondary particles are produced with significant transverse momentum and hence the hadronic showers tend to be more spread out laterally than electromagnetic showers. Long tails are present in the pion distributions. As a consequence, hadronic shower detectors must be deeper than electromagnetic detectors of the same type to completely contain the shower. Another important characteristic of a hadronic shower is that it takes longer to develop than an electromagnetic one.

The mean depth of the hadronic shower energy deposition may be parameterised as

$$\lambda_{\max} = 0.90 + 0.36 \ln E\,, \tag{1.53}$$

where $\lambda_{\max}$ is in interaction lengths and E is in GeV.

Consider the integral energy deposition. Define L to be the thickness of absorber beyond which only 10% of the energy remains. Up to 40 GeV essentially all the shower energy is contained in the first five interaction lengths. The data can be parameterised by

$$L = -1.26 + 1.74 \ln E\,, \tag{1.54}$$

where L is in interaction length and E is in GeV.

The shower grows wider as it develops due to large angle nuclear processes and multiple scattering. If only nuclear processes were involved, we would expect the shower width to steadily increase until the energy of the shower particles falls below the cutoff, at which point the shower would peter out. Actually, the width of the shower grows at first and then contracts. The narrower profiles deep in the shower are believed to be due to late developing electromagnetic processes, which tend to be produced at small angles.

The shower envelope can be defined to be the width that contains 99% of the shower energy. The width of the envelope increases slowly with energy

$$W(E) = -17.3 + 14.3 \ln E\,, \tag{1.55}$$

were the width is in centimetres and the energy is in GeV.

1.6 Problems

1. Show that the maximum energy transfered to an electron of mass m_e at rest by a much heavier particle of mass M and kinetic energy E in elastic scattering is $4Em_e/M$, or about 1/500 for protons.

2. Write the Bethe-Bloch equation in terms of dv/dx.

3. Derive a low-energy approximation for $T_{\max}$ and state the condition for validity. For a pion in copper, what error does this approximation introduce into dE/dx at 100 GeV. Answer: 6%.

4. In the minimum ionisation region where $\beta\gamma \approx 3-4$, the minimum value of $-dE/dx$ can be calculated from the Bethe-Bloch formula and for a particle with unit charge is given approximately (in units of MeV g^{-1} cm^2) by

$$\frac{1}{\rho}\left(-\frac{dE}{dx}\right)_{\min} \approx 3.5\frac{Z}{A} \text{ MeV g}^{-1} \text{ cm}^2\,. \tag{1.56}$$

5. What is the expected mean energy loss of 50 GeV protons in beryllium? How much is this result affected by density effect corrections?

6. The average number $\bar{n}$ of ionising collisions suffered by a fast particle of charge ze in traversing an interval dx (g cm^{-2}) of a medium, and resulting in energy transfer $E' \to E' + dE'$, is

$$\bar{n} = f(E')dE'dx = \frac{2\pi z^2 e^4 N_0 Z}{mv^2 A}\frac{dE'}{(E')^2}\left(1-\beta^2\frac{E'}{E'_{\max}}\right)dx\,, \tag{1.57}$$

where the symbols are the usual and the maximum transferable energy is $E'_{\max} = 2mv^2/(1-\beta^2)$. For individual particles, the distribution in number of collisions n follows the Poisson law, so that $\langle(n-\bar{n})^2\rangle$. If we multiply the above equation by $(E')^2$ and integrate, we obtain the mean squared deviation in energy loss, $\epsilon^2 = \langle(\Delta E - \overline{\Delta E})^2\rangle$, about the mean $\overline{\Delta E}$. Show that

$$\epsilon^2 = 0.6\frac{Z}{A}(mc^2)^2\gamma\left(1-\frac{\beta^2}{2}\right)\delta x\,. \tag{1.58}$$

7. Derive

$$\left(\frac{\Delta E}{\Delta x}\right)_{\min} = \frac{E_c}{X_0} \approx 3\frac{Z}{A}\frac{MeVcm^2}{g}\,. \tag{1.59}$$

Calculate the fractional rms deviation $\epsilon/\overline{\Delta E}$ in energy loss for protons of kinetic energy 500 MeV traversing (1) 0.1, (b) 1.0, and (c) 10 g cm^{-2} of plastic scintillator ($Z/A = 0.5$). Take dE/dx as 3 MeV g^{-1} cm^2.

8. For highly relativistic velocities, the energy loss of electrons is

$$-\frac{dE}{dx} = K\left(\frac{Z}{A}\right)\left(\frac{z}{\beta}\right)^2\left[\ln\frac{2mc^2}{I} - \frac{3}{2}\ln(1-\beta^2)^{1/2} - \frac{1}{2}\ln 8 + \frac{1}{16}\right] \tag{1.60}$$

whereas for protons it is

$$-\frac{dE}{dx} = K\left(\frac{Z}{A}\right)\left(\frac{z}{\beta}\right)^2\left[\ln\frac{2mc^2}{I} + 2\ln\frac{1}{(1-\beta^2)^{1/2}} - 1\right]. \tag{1.61}$$

At equal values of β, how much do the two expressions differ and over what energy range?

9. Show that a deuteron of energy E has twice the range of a proton of energy $E/2$.

10. A gamma ray is Compton-scattered backward ($\theta = 180$ deg). Calculate the energy of the scattered quantum for a primary quantum having $\hbar\omega = 0.01$, 0.1, 1.0, 10, 100, 1000 MeV.

11. Derive

$$N \approx 2^t \tag{1.62}$$

and

$$E(t) \approx \frac{E_0}{2^t}. \tag{1.63}$$

starting with an electron rather than a photon.

12. A narrow pencil beam of singly charged particles of momentum p, travelling along the x-axis, traverses a slab of material s radiation lengths in thickness. If ionisation loss in the slab may be neglected, calculate the rms lateral spread of the beam in the y-direction, as it emerges from the slab. [Hint: consider an element of slab of thickness dx at depth x, and find the contribution $(dy)^2$ which this element makes to the mean squared lateral deflection; then integrate over the slab thickness.] Use the formula you derived to compute the rms lateral spread of a beam of 10 GeV muons in traversing a 100 m pipe filled with (a) air, (b) helium, at NTP.

13. Extensive air showers in cosmic rays contain a "soft" component of electrons and photons, and a "hard" component of muons. Suppose the central core of a shower, at sea level, contains a narrow, vertical, parallel beam of muons of energy 1 TeV, which penetrate underground. Assume the ionisation loss in rock is constant at 2 MeV g^{-1} cm^2. Find the depth in rock at which the muons come to rest, assuming the rock density to be 3.0. Using the formula of the preceding problem, estimate their radial

spread in meters, taking account of the change in energy of the muons as they traverse the rock. (Radiation length in rock = 25 g cm^{-2}.)

Chapter 2

Sampling Calorimeters

Conceptually, a calorimeter is a block of matter which intercepts the primary particle, and is of sufficeint thickness to cause the particle to interact and deposit all its energy inside the detector volume in the subsequent cascade or shower of increasingly lower-energy particles. Eventually, most of the incident energy is dissipated and appears in the form of heat. Some (usually a very small) fraction of the deposited energy is detectable in the form of a more practical signal (e.g., scintillation light, Cherenkov light, or ionisation charge), which is proportional to the initial energy. Once properly calibrated, they measure the energy of the shower and hence that of the incident particle.

Calorimeters offer many attractive capabilities:

1. Sensitive to charged and neutral particles (neutral particles can only be detected in calorimeters).

2. Energy degradation through the development of the particle cascade is a statistical process, and the average number N of secondary particles is proportional to the energy of the incident particle. In principle, the uncertainty in the energy measurement is governed by statistical fluctuations of N, and hence the realtive energy resolution σ/E improves as $1/\sqrt{N} \sim E^{-1/2}$.

3. The length of the detector scales logarithmically with particle energy.

4. With segmented detectors, information on the shower development allows precise measurements of the position and angle of the incident particle.

5. Different response to electrons, muons, and hadrons can be exploited for particle identification.

6. Fast time response allows operation at high particle rates, and the pattern of energy deposition can be used for rapid online event selection.

Neutrinos, which experience only the weak interaction, pass through any calorimeter with no signal. Muons do not produce electromagnetic showers due to their high mass and also pass through without interaction.

There are homogeneous and sampling calorimeters. In a homogeneous calorimeter the entire volume is sensitive, i.e. contributes signal. Homogeneous calorimeters (usually electromagnetic) may be built with inorganic heavy (high-Z) scintillating crystals such as bismuth germanate (BGO), CsI, NaI, and PWO; non-scintillating Cherenkov radiators such as lead glass and lead fluoride; thallium-doped heavy liquid counters; or ionising noble liquids. The best resolutions are obtained with an organic scintillating crystal. Lead glass counters detect the Cherenkov light of shower electrons, the resolution is limited by photoelectron statistics.

A sampling calorimeter consists of an active medium which generates signal and a passive medium which functions as an absorber. The active medium may be a scintillator, an ionising noble liquid, a gas chamber, a semiconductor, or a Cherenkov radiator. The passive medium is usually a material of high density, such as lead, iron, copper, or depleted uranium.

Sampling calorimeters are devices in which the flucturations of energy degradation and energy measurement are separated in alternating layers of different substances. This allows a considerably greater freedom in the optimisation of detectors for certain specific applications. The choice of passive absorber – typically plates made of Fe, Cu, or Pb each ranging in thickness from a fraction of X_0 to a few X_0 – makes possible to build rather compace devices, and it permits optimisation for a specific experimental requirement such as electron/pion discrimation or position measurement. Independently of the choice of the absorber, the readout method may be selected for best uniformity of signal collection, high spatial subdivision, rate capability, or other criteria. The disadvantage is that only a fraction of the total energy of the electromagnetic cascade is sampled in the active planes, resulting in additional sampling fluctuations of the energy determination.

A calorimeter is designed to measure the energy deposited in a contained electromagnetic (EM) or hadronic shower. The characteristic interaction distance for an electromagnetic interaction is the radiation length X_0, which ranges from 13.8 g cm^{-2} in iron to 6.0 g cm^{-2} in uranium. Similarly, the characteristic nuclear interaction length λ_I varies from 132.1 g cm^{-2} (Fe) to 209 g cm^{-2} (U). This scale is big in comparison with the radiation length X_0 for heavy elements, so that, in comparison with electromagnetic shower detectors, hadron calorimeters are large. In either case, the calorimeter must be many interaction lengths deep, where "many" is determined by physical size, cost, and other factors. EM calorimeters tend to be 15-30 X_0 deep, while hadronic calorimeters are usually compromised of 5-8 λ_I. Moreover, in a real experiment there is likely to be an EM calorimeter in front of the hadronic section, and perhaps a more poorly sampling catcher in the back, so the hadronic cascade is contained in a succession of different structures. In all cases there is a premium on high density, to contain the shower as compactly as possible, and, especially in the EM case, high atomic number. Calorimeters are known as destructive detectors.

We first study the principles freatures of detector designed to measure the energy of photons and electrons, the electromagnetic shower detectors. Secondly we study the physics of hadronic calorimeters. The final study is the information processing from calorimeters. We end with a discussion of the state-of-the-art Monte Carlo simulation of electromagnetic and hadronic showers. Will not discuss total absorption Cherenkov detectors or air-shower Cherenkov detectors.

Ideally, the calorimeter is segmented in ϕ, and θ or $\eta = -\ln\tan(\theta/2)$. Fine segmentation, while desirable, is limited by cost, readout complexity, practical geometry, and the transverse size of the cascades.

2.1 Electromagnetic Shower Detectors

Electromagnetic calorimeters use electromagnetic showers to detect electrons and photons. Some electromagnetic sampling calorimeters constructions are

1. metal-scintillator sandwich,
2. metal-liquid argon ionisation chamber,
3. metal-gaseous PWCs.

Each device consists of alternate layers of metal radiator to enhance photon conversions and some active substance to sample the energy loss. The metal radiator is usually made of lead. The calorimeter cells are typically arranged in either a strip or a tower arrangement. In a strip structure, the profile of the shower is sampled at various depths. Usually two or three profile orientations are measured. In a tower structure the calorimeter is divided into many narrow, deep units that point to the interaction region.

In the scintillator device, charged particles in the shower produce light in the scintillator planes. Both solid and liquid scintillator have been used. The signal produced is usually large and very fast, making it useful in a high rate environment. Problems arise when the detector must be finely segmented or operated inside a magnetic field. The photomultiplier tube (PMT) must be located in a weak field, and this may require a complicated light pipe system. The signal from the PMT is usually fed into an ADC, which gives an output proportional to the area under the PMT signal.

A liquid argon calorimeter consists of a series of metal plates immersed in liquid argon. The plates are maintained at a positive high voltage so that electrons produced in the liquid argon are collected at the plates. Since there is no charge multiplication, the collected charge is quite small and the detector requires a preamplifier and associated electronics for each channel. The chamber must be operated at liquid argon temperatures (80 K) and thus requires a cryogenic system. The detector is relatively slow. On the other hand, it is stable, is not adversely affected by the presence of a magnetic field, and is easily segmented. The detector has uniform sensitivity, and it is possible to make a highly accurate charge calibration.

2.1.1 Energy Loss Mechanism

Above energies of approximately 1 GeV, the principle processes – bremsstrahlung for electrons and positrons, and pair production for photons – become energy independent. It is through a sucession of these energy loss mechanisms that the electromagnetic cascade is

propagated, until the energy of the charged secondaries has been degraded to the regime dominated by ionisation loss. Within this description, the combined energy loss of the cascade particles in the detector equals the energy of the incident electron or photon. The measureable signal – excitation or ionisation of the medium – can be considered as the sum of the signals from the track segments of the positrons and electrons, see Fig. 2.1.

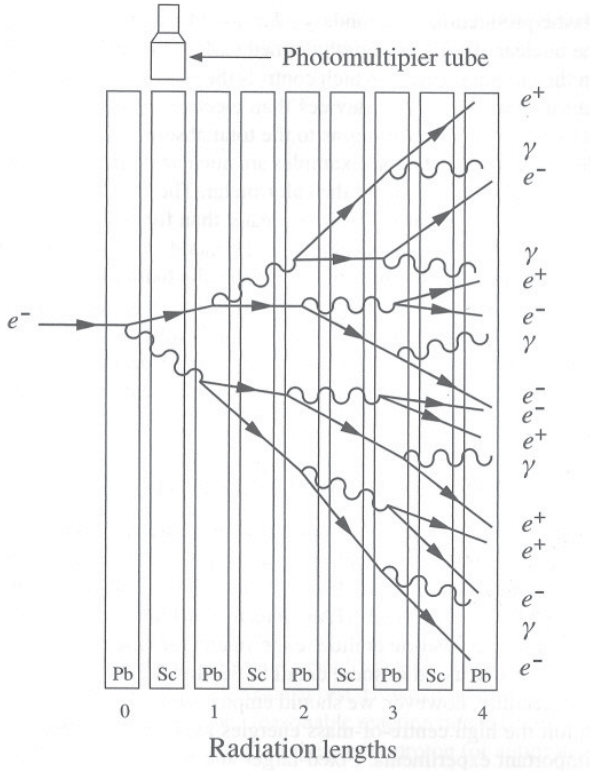

Figure 2.1: Approximate development of an electromagnetic shower in a sampling calorimeter assuming the simple model of the notes. The calorimeter consists of alternating layers of lead (Pb) and a scintillator (Sc), the later attached to photomultipliers (one only shown).

It is possible to describe the characteristic longitudinal dimensions of the high-energy electromagnetic cascade ($E > 1$ GeV) in a material-independent way, using the radiation length X_0. The energy loss ΔE by radiation in length Δx can be written

$$(\Delta E)_{\text{radiation}} = -E\frac{\Delta x}{X_0} \tag{2.1}$$

and the numerical value is well approximated by the following expression: X_0 [g/cm^2] $\approx 180A/Z^2$ (to better than 20% for approximately $Z > 13$).

While the high-energy part of the electromagnetic shower part of the electromagnetic cascade is goveerned by the value of X_0, the low-energy tail of the shower is characterized by

the critical energy E_c of the medium. It is defined as the energy loss by collison of electrons or positrons of energy E_c in the medium in one radiaition length, i.e.,

$$(dE)_{\text{collision}} = -E_c \frac{dx}{X_0}\,, \tag{2.2}$$

where E_c (MeV) $= 800Z^{-1}$.

This value of E_c coincides approximately with that value of the electron energy below which the ionisation energy loss starts to dominate the energy loss by brensstrahlung. The critical energy E_c is seen to define the dividing line between shower multiplication and the subseqent dissipation of the shower energy through exication and ionisation.

The most useful features describing the logitudinal shower profile are

1. The cross section for ionisation is energy independent, i.e., $dE/dx = -E_c/X_0$.
2. Multiple scattering is neglected and the electromagnetic cascade is treated in one dimension.
3. Compton scattering is neglected.

The transverse shower properties can be understood qualitatively as follows. In the early, most energetic part of the cascade the lateral spread is characterised by both the typical angle for bremsstrahlung emission $\theta_{\text{brems}} \sim p_e/m_e$ and multiple scattering in the absorber. This latter precess incrasingly influences the lateral spread with decreasing energy of the shower particles and causes a gradual widening of the shower. For the purpose of total energy measurements, the electromagnetic cascade occupies a cylinder of radius $R = rR_M$, where

$$R_M = 21\frac{X_0}{E_c} = 7\frac{A}{Z}\ [\text{g cm}^{-2}] \tag{2.3}$$

is the Moliere radius, which describes the average lateral deflection of electrons of energy E_c after traversing one radiation length. The factor of 7 is when $E_c = 550$ MeV$/Z$. The transverse shower profile as a function of depth exhibits the rather pronounced central and energetic core surrounded by a low-energy halo.

2.1.2 Energy Resolution in Sampling Calorimeters

The final signal from any detector is the number of electrons that are registered in the electronic circuits. The resolution of the device for detecting an incident particle of energy E_0 is determined by fluctuations in the number N of these electrons. The fluctuations can arise from

1. the actual energy deposited in the active layers of the detector (sampling fluctuations),
2. leakage of energy out of the calorimeter,
3. noise in the active layers,

4. photocathode statistics or gain variations,

5. electronic noise, and

6. more than one event within the time resolution (pileup).

The major contribution to the energy resolution of electromagnetic calorimeters is usually sampling fluctuations.

It is instructive to expand the variance of the energy distribution into a power series in E,

$$\sigma^2(E) = \sigma_0^2 + \sigma_1^2 E + \sigma_2^2 E^2 + \cdots . \tag{2.4}$$

Dividing by E^2. we obtain an expression of the energy resolution

$$\left(\frac{\sigma(E)}{E}\right)^2 = \frac{\sigma_0^2}{E^2} + \frac{\sigma_1^2}{E} + \sigma_2^2 + \cdots . \tag{2.5}$$

The constant σ_0 represents contributions to the resolution that are only important at low energy, primarily the ADC pedestal widths. The σ_1 term is usually dominant. Any process governed by Poisson statistics will contribute to this term. If these fluctuations follow a Poisson distribution, the standard deviation is $\sigma = \sqrt{N}$, and the resolution is $\sigma(N)/N = 1/\sqrt{N}$. These include fluctuations in energy loss (sampling) and fluctuations in the number of photoelectrons released at the face of a PMT. Contributions to σ_2 affect the resolution curve as a whole. Hence they include calibration errors.

The energy resolution σ_E/E of a sampling calorimeter can be parameterised as

$$\frac{\sigma_E}{E} = \frac{a}{\sqrt{E}} \oplus b \oplus \frac{c}{E}\,, \tag{2.6}$$

where $\oplus$ represents addition in quadrature and E is in GeV.

The stochastic term a represents statistics-related fluctuations such as intrinsic shower fluctuations, photoelectron statistics, dead material at the front of the calorimeter, and sampling fluctuations. For a fixed number of radiation lengths, the stochastic term a for a sampling calorimeter is expected to be proportional to $\sqrt{t/f}$, where t is the plate thickness and f is sampling fraction. While a is at few percent level for a homogeneous calorimeter, it is typically 10% for sampling calorimeters.

The energy resolution of an idealised homogeneous detector of infinite dimensions is limited by statistical fluctuations. If the shower is not contained in the detector, the fluctuation of the energy leaking out gives a contribution to the resolution.

The main contributions to the systematic, or constant, term b are detector non-uniformity and calibration uncertainty. A homogeneous detector is very important to avoid non-uniformity in the signal collection. In the case of hadronic cascades non-compensation also contributes to the constant term. One additional contribution to the constant term for calorimeters built for modern high-energy physics experiments, operating in a high-beam

intensity environment, is radiation damage of the active medium. With effort, the constant term b can be reduced to below one percent.

The term c is due to electronic noise summed over readout channels within a few Moliere radii.

These general comments apply to both electromagnetic and hadronic calorimeters. The following discussion of sampling fluctuations is specifically valid for the measurement with electromagnetic calorimeters, for which sampling fluctuations have been rather carefully studied. We know that they depend on the characteristics of both the passive and the active medium (in particular, thickness and density) and that several effects contribute to the total sampling fluctuation.

The principle contributions to the energy resolution in electromagnetic calorimeters is as follows.

1. Intrinsic shower fluctuations. Track-length fluctuations: $\sigma/E \gtrsim 0.005/\sqrt{E}(GeV)$.

2. Sampling fluctuations. $\sigma/E \approx 0.04\sqrt{\Delta E/E}$. Nature of readout may augment sampling fluctuations.

3. Instrumental effects. Noise and pedestal width: $\sigma/E \sim 1/E$ – determine minimum detectable signal; – limit low-energy performance. Calibration errors and non-uniformities: $\sigma/E \sim$ constant and therefore limits high-energy performance.

4. Incomplete containment of shower. $\sigma/E \sim E^{-\alpha}, \alpha < 1/2$. For leakage fraction $\geq$ few %: non-linear response and non-Gaussian 'tail'.

The energy resolution of an idealised homogeneous detector of infinite dimensions is limited only by statistical fluctuations. For a cut-off energy of 0.5 MeV and a critical energy of 11.8 MeV, a total track length of 176 cm/GeV and a resolution of

$$\frac{\sigma(E)}{E} = \frac{0.7\%}{\sqrt{E(\mathrm{GeV})}} \tag{2.7}$$

has been computer.

The intrinsic sampling fluctuations express the statistical fluctuations in the number of electron-positron pairs traversing the active signal planes and can be estimated. The contribution to the energy resolution is

$$\frac{\sigma(E)}{E_{\mathrm{sampling}}} = 3.2\%\sqrt{\frac{\Delta E}{E}}\,. \tag{2.8}$$

This experession has to be regarded as a lower bound on the sampling fluctuations.

To these two sources of fluctuations, valid for homogeneous calorimeters, we have to add the sampling fluctuations if the shower calorimeter consists of a series of inactive absorber layers of thickness d interspersed with active detector layers ("sampling calorimeter"). If the detectors count only the number of particle traversals, N, the statistical fluctuation in N

determines the contribution to the energy resolutions. Since N depends on the total track length, $N = S/d = E_0 X_0 F(z)/(E_c d)$ we obtain

$$\frac{\sigma(E)}{E_{\text{sampling}}} = \frac{1}{\sqrt{N}} = 3.2\%\sqrt{550}\,. \tag{2.9}$$

Another large source of fluctuations enters if the sensitive layers of the calorimeter consist of gas or a very thin layer of liquid argon, used in proportional counters. Then low energy electrons moving at large angles relative to the shower axis induce large pulse-height fluctuations ("path length fluctuations"), and the Landau tail of the energy loss distribution also leads to a reduction of resolution.

In high Z materials, the lateral dimension of the showers is much larger than in those with low Z, since the Moliere radius in units of X_0, $R_M/X_0 = 21$ MeV$/E_c$, is larger for heavy materials. Consequently also the angle θ of electrons and positrons relative to the shower axis is larger. Those shower particles see a larger sampling thickness $d/\cos\theta$, and therefore a smaller number of traversals occurs, reducing further the energy resolution by a factor $\langle\cos\theta\rangle^{-1/2}$.

We can represent the track length T by

$$T(X_0) = \frac{E_{\text{particle}}}{E_c}\,. \tag{2.10}$$

The detectable track length T_d, i.e., the equivalent track length which corresponds to the measured signal in a particualr detector, will in geneal be shorter, $T_d \leq T$, as practical devices are only sensitive to the cascade particles above a certain threshold energy η. The average detectable track length is $\langle T_d\rangle$, and calorimetric energy measurments are possible because $\langle T_d\rangle \propto E$ for any reasonable value of E_c. The resolution of the energy measurement is determined by the fluctuations in the shower propagation. The intrinsic component of the resolution is caused by the fluctuations in T_d. This represents the lower bound on the resolution and may be qualitatively estimated in the following way: the maximum number of track segments is $N_{\max} = E/\eta$ hence $\sigma(E)/E \geq \sigma(N_{\max})/N_{\max}$.

2.1.3 Position and Angular Resolution

The impact point of an electron or photon on an array of shower counters can be obtained by measuring the lateral distribution of energy in the shower. The position resolution depends on the effective Molière radius and the transverse granularity of the calorimeter. The precision of the position information increases with the number of cells hit by shower particles, and decrease with the cell size. Particularly, the accuracy is best if the shower energy is shared equally between two adjacent cells.

Like the energy resolution, position resolution can be factored as $a/\sqrt{E} \oplus b$, where a is a few to 20 mm and b can be as small as a fraction of mm for dense calorimeters with fine granularity.

Electromagnetic calorimeters may also provide direction measurements for electrons and photons. Typical photon angular resolution is about 45 mrad$/\sqrt{E}$, which can be provided by

implementing longitudinal segmentation for a sampling calorimeter or by adding a preshower detector for a homogeneous calorimeter without longitudinal segmentation.

2.2 Hadronic Shower Detectors

Conceptually, the energy measurement of hadronic showers is analogous to that of electromagnetic cascades, but the much greater variety and complexity of the hadronic processes propagating the hadronic cascade complicate the detailed understanding. No simple analytical description of hadronic showers exists, but the elementary prcesses are well studied.

Most large hadron calorimeters are sampling calorimeters which are parts of complicated 4π detectors at colliding beam facilities. Typically, the basic structure is plates of absorber (Fe, Pb, Cu, or occasionally U or W) alternating with plastic scintillators (plates, tiles, bars), liquid argon (LAr), or gaseous detectors. The ionisation is measured directly, as in LAr calorimeters, or via scintillation light observed by photodetectors (usually PMT's). Waveshifting fibres are often used to solve difficult problems of geometry and light collection uniformity.

The scale for the spatial development of a hadronic shower, the inelastic production of secondary hadrons, which again interact inelastically producing tertiary hadrons, and so one, is given by the nuclear absorption length λ. The experimental values of λ for materials usable for calorimetry are 77 g/cm^2(C), 135 g/cm^2(Fe), 210 g/cm^2(Pb), and 227 g/cm^2(U). Compared to the small values for the radiation length of high Z materials enabling the construction of correspondingly small show counters, the size of hadronic showers is large; typical values for Fe calorimeters are 2 m depth and 0.5 m transverse size. In general, one wants a high density since the shower depth is roughly inversely proportional to ρ. The energy resolution improves with the use of uranium plates. The reason for this seems to be related to the conversion of incident energy into binding energy in nuclear interactions. This energy is ordinarily not detected.

Homogeneously active devices have been used in many paractical applicaions for the measurement of electromagnetic showers. Sampling devices represent the only really practical form of hadronic calorimeters.

2.2.1 Energy Resolution

In general, the energy resolution of hadron calorimeters is worse than theat of electromagnetic calorimeters. Hadronic calorimeters are subject to all the fluctuation in connection with electromagnetic calorimeters and to additional fluctuations due to nuclear interactions. The energy used for the production of neutrinos and high energy muons and binding energy losses represents energy that escapes from the calorimeter. Fluctuations in the importance of these processes represent a major contribution to the energy resolution of these processes represent a major contribution to the energy resolution of hadron calorimeters.

Fluctuations in the hadronic development, producing a range of different particles with vastly different detection characteristics, are the principle limitations to the energy resolu-

tions. These fluctuations have been found to be large, of the order of 50% at 1 GeV – in strong contrast with the measurement of electromagnetic calorimeters, where the intrinsic fluctuations of the visible track length are less than 1% at 1 GeV.

Average longiudinal and transverse distributions are useful esimates of the characteristic dimensions for near-complete shower containment. The average longitudinal distribution exhibits scaling in units of absorption length λ. The transverse distributions depend – as in the case of electromagnetic cascades – on the longitudinal depth: the core of the shower is rather narrrow, increasing with shower depth. The highly energetic, very collimated core is surrounded by lower-energy particles, which extend a considerable distance away from the shower axis, such that for 95% containment a cylinder of radius $R \sim 1\lambda$ is required.

Typical of hadronic interactions is multiple particle production with transverse momentum $\langle p_{\mathrm{T}} \rangle \approx 0.35$ GeV, for which about half of the available energy is consumed. The remainder of the energy is carried by fast, forward-going (leading) particles. The secondaries are mostly pions and nucleons, and their multiplicity is only weakly energy-dependent. Two specific features have been identified as the principle physics limitations to the energy resolution of hadronic calorimeters:

1. A considerable part of the secondaries are neutral pions, which will propagate electromagnetically without any further nuclear interactions. The size of the neutral pion component is largely determined by the production in the first interaction, and event-by-event fluctuations about the average value are important.

2. A sizable amount of the available energy is converted into excitation or break-up of the nuclei, of which only a fraction will result in detectable (visible) energy.

3. Muons and neutrinos will be lost in the form of invisible or undetected energy.

Apart from the hardon shower particles leaking out longitudinally or laterally, the energy seen in a sampling calorimeter for hadrons is incomplete for several reasons:

1. there are particles escaping the calorimeter carrying away energy, like muons and neutrinos from pion decay.

2. There is nuclear excitation and breakup resulting in low energy gamma-rays or heavy fragments which do not reach the sensitive part of the sandwich.

The principle contributions to the energy resolution in electromagnetic calorimeters is as follows.

1. Intrinsic shower fluctuations. Fluctuations in the energy loss: $\sigma/E \gtrsim 0.45/\sqrt{E}(\mathrm{GeV})$. Scaling weaker than $1/\sqrt{E}$ for high energies. With compensation for nuclear effects: $\sigma/E \approx 0.22/\sqrt{E}(\mathrm{GeV})$.

2. Sampling fluctuations. $\sigma/E \approx 0.09\sqrt{\Delta E/E}$.

3. Instrumental effects. Noise and pedestal width: $\sigma/E \sim 1/E$ – determine minimum detectable signal; – limit low-energy performance. Calibration errors and non-uniformities: $\sigma/E \sim$ constant and therefore limits high-energy performance.

4. Incomplete containment of shower. $\sigma/E \sim E^{-\alpha}, \alpha < 1/2$. For leakage fraction $\geq$ few %: non-linear response and non-Gaussian 'tail'.

Experimental evidence indicates that the intrinsic hadronic energy resolutions is

$$\left(\frac{\sigma(E)}{E}\right)_{\text{intrinsic}} \approx \frac{45\%}{\sqrt{E}(\text{GeV})}\,. \tag{2.11}$$

This relation describes devices make from materials covering almost the complete periodic table from aluminium to lead. Besides hydrogen, the sole known exception from this rule is give by uranium-238, for reasons that we shall explain.

On top of this fluctuation there is the sampling fluctuation which alone gives rise to a resolution about twice as large as in electromagnetic showers. However, the effects of fluctuations in energy leakage and in the electromagnetic component of the hadronic shower are much larger here.

Most hadronic calorimeters are sampling detectors using preferentially rather dense passive absorbers to reduce the linear dimensions of the instrument. As a consequence, sampling fluctuations of statistical origin may contribute to the energy resolution. Hadronic sampling fluctuations are approximatley twice as large as the electromagnetic sample fluctuations for the same detector; unlike the electromagnetic case, where sampling is the predominant contribution to the resoluiton, sampling in hadronic detectors can be made small relative to the large intrinsic component, and energy resolution need not be sacrificed in hadronic sampling calorimeters.

The fluctuations in the hadronic cascade development producing a range of different particles – from neutral pions to slow neutrons, muons and neutrinos – with vastly different detection characteristics, are the principle limitatons to the energy resolutions. These fluctuations have been found to be large – of the order of 50% at 1 GeV – in strong contrast with the measurement of electromagnetic calorimeters, where the intrinsic fluctuations of the visible track length are less thant 1% at 1 GeV.

The two processes, intimately correlated may lead for a given entering hadron to a very different shower composition, which has a very different detectable response. Together they impose the intrinsic limitation on the performance of hadronic calorimeters.

Leakage

Energy leakage due to partial shower containment will not only degrade the energy resolution, but will also give rise to a very asymmetric resolution functions with low-energy tails. Calorimeter experiments, which emphasize meaurements such as neutrino detection based on missing energy or hadronic high-p_{T} jet production have therefore particularly stringent requirements to achieve very close to 100% containment. Longitudinal fluctuations are larger

than transverse fluctuations and hence longitudinal leakage is more critial to the performance. In practical detectors, usually a number of additional components must be considered, which may conspire to affect the resolution. One important instumental contribution to the energy resolution comes from incomplete containment of the showers (energy leakage). Longitudinal leakage is more critical than transverse leakage due to the fact that fluctuations about the average longitudinal loss are much larger than for transverse leakage.

Although the total depth needed for near-complete abosorption increases only logarithmically with energy, it does require, for example, about 8λ to contain on average more than 95% of a 350 GeV pions.

The discussion above assumes an idealised calorimeter with the same structure throughout and without leakage. "Real" calorimeters usually have an EM detector in front and a coarse "catcher" in the back. Complete containment is generally impractical.

Two ways of improving this resolution have been invented and tried out successfully: 1) The loss of visible energy through the nuclear excitation and breakup mechanism can be nearly completely compensated by the energy release in nuclear fission of uranium-238. Energetic photons from the fission contribute to the observed signal such that the pulse height from hadron showers becomes nearly equal to the one from electromagnetic showers. The corresponding fluctuations disappear, and the energy resolution decreases by about a factor of two. 2) Another method reduces the fluctuations due to the electromagnetic component by weighting the response in individual counters. Electromagnetic parts of the shower are localized, therefore producing very large depositions in individual counters.

2.2.2 Compensation

In an inelastic hadronic collision a significant fraction f_{em} of the energy is removed from further hadronic interaction by the production of secondary π^0's and η's, whose decay photons generate high-energy EM cascades. Charged secondaries ($\pi^{\pm}$, p, ...) deposit energy via ionisation and excitation, but also interact with nuclei, producing spallation protons and neutrons, evaporation neutrons, and recoiling nuclei in highly excited states. The charged collision products produce detectable ionisation, as do the showering γ-rays from the prompt de-excitation of highly excited nuclei. The recoiling nuclei generate little or no detectable signal. The neutrons lose kinetic energy in elastic collisions over hundreds of ns, gradually thermalise and are captured, with the production of more γ-rays – usually outside the acceptance gate of the electronics. Between endothermic spllation losses, nuclear recoils, and late neutron capture, a significant fraction of the hadronic energy (20%-35%, depending on the absorber and energy of the incident particle) is invisible.

In contrast to EM showers, hadronic cascade processes are characterised by relatively few high-energy particles being produced. The lost energy and the $\pi^0 \rightarrow \gamma\gamma$ fraction f_{em} are highly variable from event to event. Until there is event-by-event knowledge of both the invisible energy loss and the EM deposit, the energy resolution of a hadron calorimeter will remain significantly worse than that of an EM calorimeter.

The EM energy deposit is usually detected more efficiently than the hadronic energy deposit. If the detection efficiency for the EM sector is e and that for the hadronic sector is

h, then the ratio of the mean response to a pion to that for an electron is

$$\frac{\pi}{e} = \langle f_{em} \rangle + \langle f_h \rangle \frac{h}{e} = 1 - \left(1 - \frac{h}{e}\right) \langle f_h \rangle \approx 1 - \left(1 - \frac{h}{e}\right) \left(\frac{E}{E_0}\right)^{m-1} . \qquad (2.12)$$

If $h \neq e$, the hadronic response is not a linear function of energy.

For $h/e \neq 1$, fluctuations in f_{em} significantly contribute to the resolution, in particular contributing a large fraction of the variance at high energies. Since the f_{em} distribution has a tail on the high side, the calorimeter response is non-Gaussian with a high-energy tail if $h/e < 1$. Noncompensation ($h/e \neq 1$) thus seriously degrades resolution as well as producing a nonlinear response. It is clearly desirable to compensate the response, i.e. to design a calorimeter such that $h/e = 1$. This is possible only in a sample calorimeter, where several variables can be chosen or tuned.

The relative response between electrons and pions is a senstive measure of the level of nuclear interactions. An improvement in the energy response would be expected if the response of the electromagnetic cascade were idential compared with the purely hadronic one, i.e., if devices with an e/h ratio equal to one were available. Alternatively, given sufficiently detailed information on the individual hadronically induced shower, one would be able to access the relative components and apply suitable corrections to improve the energy resolutions.

Consider equalising the response for electrons and hadrons. In principle, equalisations of these differences, which are at the 30% to 40% level, may be accomplished in two ways: either by decreasing the electron response – typally 20% to 40% lower relative to a minimum-ionising particle calibration, or by boosting the hadronic signal. This latter aspect is being exploited by using uranium-238 as the energy degrader. In that material (and probably also to a lesser extent in thorium) some of the normally invisible energy expanded in the nuclear break-up leads to neutron-induced fission, which in turn produces detectable energy in the calorimter. One may achieve essentially complete compensation not only on average but also event-by-event. The intrinsic resolution is measured to be

$$\left(\frac{\sigma(E)}{E}\right)^{\text{uranium}}_{\text{intrinsic}} \approx \frac{22\%}{\sqrt{E}(\text{GeV})} . \qquad (2.13)$$

The fundamental importance of equalising the hadronic and electromagentic resonse should again be emphasised. The latter sensitively depends on the details of the low-energy part of the electromagnetic cascade and hence critically on the material and the sampling fequency. It would appear that this is one further contribution to the tuning of the e/h ratio. Hence for hadron showers, the level of visible compensation is expected to be affected not only by the choice of the passive absorber but also by the response of the active readout to densely ionising particles (from the hadronic cluster) and to the electromagnetic component.

2.2.3 Spatial Resolution for Hadronic Showers

Position and angular resolution depend on the degree of segmentation of the active regions. Fine segmentation is necessary to reduce the ambiguity in multiparticle events or to separate nearby showers. This is particularly important for π^0 identification.

Hadron showers are found to consist of a narrow core surrounded by a halo of particles extending to several times the dimensions of the core. Consequently, somewhat different criteria apply to the measurement of the position and to considerations of shower separation.

2.2.4 Calorimeteric Energy Resolution of Jets

The physics emphasis is shifting from the measuremnt of single particles to the analysis of jets of hadrons considered as the principle manifestation of quarks and gluons. Studies are done largely through the invariant mass determination of multijet systems. There are two distinct contributions to the resolution of this invariant mass determination. The first effect is associated with the physics of jet production. Jets, unlike single particles, are not unambiguously defined objects, but have to be defined operatinally by a jet algorithm. For example, hadron-initiated jets are produced together with particles originating from peripheral interactons; multijets may partially coalesce. The second contribution to the mass resolution depends on the calorimeter preformance itself, and in particular on the momentum response to different particles. For very low energies of the jets, the jet resolution is dominated by the very non-linear response to low-momentum particles, and is similar for both calorimeters. At very high energies, the performance is dominated by the relative electron/hadron response.

A similar argument should also be valid for single, very energetic hadrons, which after the first inelastic interaction in a calorimeter will be similar to a jet of particles of comparable energy.

2.2.5 Particle Identification

With hadronic calorimters it is possible to identify a class of particles which are not always identified by other methods.

Descrimination between Electrons (Photons) and Hadrons

The discrimination between electrons or photons and hadrons is based on the difference in the shower profiles, accentuated in materials with very different radiation and absorption lengths. Heavy materials (lead, tungsten, or uranium) are best suited for electron-hadron discrimination.

Muon Identification

Several calorimetric methods exist for discriminating between muons, and hadrons or electrons. All are based on the very large difference in the energy deposits.

1. Calorimters with fine longitudinal subdivision: such calorimeters, are typically many tens of absorption lengths long. Energetic muons are very clearly recognised as isolated, minimum-ionising tracks, frequently ranging far beyond the tracks from hadronic showers.

2. Muon penetraton through active or passive absorbers: the absorbers or calorimters are deep enough to contain the hadrons adqueately and to reduce the punch through probability of pions. The detailed rejection power against hadrons depends critically on the experimental precautions taken and may be improved by:

   (a) Reducing the background from pions and kaon decay before the calorimeter; the active beam dump experiments have refined this method.

   (b) Measuring the muon momentum after the calorimeter in, for example, magnetised iron or a precision magnetic spectrometer; momentum matching of muon candidates before and after the absorber may further improve the rejection.

   (c) Correlating the direction of the particle before and behind the absorber. The applicability of the method is limited by multiple scattering of the muons in the absorber, and accidental overlap with nearby tracks before the absorber.

Neutrino Identification

Missing momentum analysis can allow us to infer the presence of neutrinos. Two related methods can be used:

1. Total ernergy measurement can be accomplished provided 4π calorimetric coverage in the centre of mass system is avaialble for all particles (charged, neutral, muons). Neutrino production is implied, whenever the measured energy is lower than the total available energy and incompatible with the resolution function of the detector. Total energy measurement does not work well at a hadron collider because a signficant fraction of the total energy is always produced at very small angles relative to the incident beams, making a calorimetric measurement impractical. Help is provided by

2. a misisng transverse momentum measurment. In this method, clearly related to method 1., the production of a neutrino is signalled by $\sum p_{\mathrm{T},i} \neq 0$ to a degree which is incompatible with the detector resolution.

2.3 Signal Readout Techniques for Calorimeters

The principle goal is to develop methods which will minimise the instrumental effects, relative to the intrinsic performance, caused by the physics of the detectors. The crieria are:

1. The response must be linear as a function of the particle energy, frequently over a very large dynamic range.

2. The noise or the non-uniformity of the readout system (photoelectron statistics, equivalent noise charge of preamplifiers) must not dominate the energy resolution.

3. The readout system must have a rate capability adapted to the observed interacton rate.

4. Provision must be made for adequate longitudinal and transverse segmentation.

5. The absolute and relative energy response must be monitored and maintained with sufficeint accuracy.

6. Other operational charactersistics, such as sensitivity to magnetic fields, radiation, and temperature have to be considered.

2.3.1 Light-collecting readout

An example of a light-collecting sampling calorimeters is plastic scintillators and light-readout techniques using wavelength shifters (WLS) to replace the technique of scintillator plates individually coupled to a light guide. Scintillation light crosses an air gap and enters the WLS, where it is absorbed and subsequently re-emitted at longer wavelengths. A fraction of this wavelength-shifted light is then internally reflected to the light detector. This scheme avoids complicated and costly optical contacts between the scintillators and the light collectors, and minimises dead space.

2.3.2 Charge collection readout

The ionisation charge produced by the passage of the charged particles of the shower may be collected from solids, liquids, or gases. Solids and liquids can only be used in an ionisation chamber mode with no internal amplification. The best known and, to date, the only practical example is based on the use of liquid argon. In specific cases, liquid xenon may be used. The use of room-temperature liquids has also been advocated, but with increased operating temperature the tolerable level of impurities decreases strongly. If gas is used as the active sampling medium, internal amplification to various degrees are usually exploited. Proportional chambers or tubes provide a signal proportional to the energy loss. The principal advantages common to all these charge collection methods are seen in the ease of segmentation of the readout and the capability to operate in magnetic fields. The calorimeter readout may be either digital or proportional.

2.3.3 Bolometric readout

Particles have been detected through the temperature rise in a calorimeter, caused by the absorption of the particles. Such experiments contributed decisively to our understanding of radioactivity and to the concept of the neutrino.

2.4 System Aspects of Calorimeters

Important aspects of calorimeter design:

1. solid angle coverage,
2. operation in a magnetic field,
3. rate characteristics,
4. position and angular resolution,
5. particle identification capability,
6. resolving time,
7. energy resolution.

2.4.1 General Scaling Laws of the Calorimeter Dimensions

A number of parameters which may be external to the calorimeter design, e.g., the dimensions of a charged-particle spectrometer, may ultimately determine the size of a calorimeter. If, however, global optimisation of an experiment is attempted, one should aim for the most compact calorimeter layout that may lead to the achievement of the physics goals of the detector.

The distance D of a calorimeter from the interaction vertex, and hence its necessary size, is determined by the achievable useful segmentation and the characteristic angular dimension θ required to be resolved in the measurement. The useful segmentation d is determined by the shower dimensions, approximately $d \sim 2R_M$ for electromagnetic detectors. and $d \sim \lambda_I$ for hadronic calorimeters. The characteristic angular dimension θ may be the minimum angular separation of the photons from neutral pion decays, or the typical angle between the energetic particles in a hadron jet.

For correctly designed detector systems, the calorimeter dimensions are determined by the angular topology and size of the showers to be measured. This minimum detector distance is then $D \geq d/\tan\theta$, and the required calorimeter volume V is found to be

$$V \propto D^2 L(\text{depth of calorimeter required for total absorption})\,, \tag{2.14}$$

whence

$$V \propto R_M^2 X_0 \text{ for electromagnetic detectors} \tag{2.15}$$

and

$$V \propto \lambda_I^2 \lambda_I \text{ for hadronic detectors}\,. \tag{2.16}$$

The third-power dependence of the calorimeter volume on shower dimensions implies that it may be economically advantageous to select very compact calorimeter designs, even if the price per unit volume is very high.

2.4.2 Monte Carlo Simulations

Formulae are given which approximately describe average showers, but since the physics of electromagnetic showers is well understood, detailed and reliable Monte Carlo simulation is possible. EGS4 and GEANT have emerged as the standards.

The relatively simple physics governing the electromagnetic showers has facilitated their Monte Calor simulation. One program has emerged at the world-wide standard for simulating electromagnetic calorimeters. The current version is EGS IV. It has successfully passed many very detailed tests.

Sophisticated Monte Carlo codes that simulate high energy hadronic showers are very useful in calorimeter design. The code takes into account relevant processes such as energy loss, particle decay, scattering, Fermi motion, neutron absorption, noise, and so on.

The physics and consequently its simulation are considerably more complex for hadronic showers. Several programs have been developed, the aim of which is to simulate fairly accurately the detailed particle production of a hadronic cascade. Even the most faithful physics simulation of the hadonic process will not guarantee unconditional success. Already the uncertainties associated with the sampling medium (relative response to minimum and heavily ionising particles) and the complexities of the nuclear interactions are too large to make a calculation possible. These programs therefore require careful tuning against many different measurements before they become a reliable guide for designing new facilities.

2.4.3 Calibration and Monitoring of Calorimeters

In a typical large-scale calorimeter there will be several thousand channels of analog pulse height information which is converted to digits and registered. A severe problem with such a number of channels is their calibration and monitoring.

The calibration can be done by using suitable hadron beams and calibrating the response of the calorimeter, where for each sampling detector the pulse height is measured in terms of minimum ionisation deposited by high energy muons.

If there are not as many muons in each sampling detector as are needed for day-to-day monitoring, another source of calibrated pulse heights is needed. For liquid argon calorimeters, such a source is obtained by depositing a known amount of charge into the ion chamber. The same can be done for proportional chambers.

2.5 Problems

1. Describe one method in detail for designing a compensating calorimeter.

2. A 50 GeV electron traverses a stack of iron. (a) Using the Heitler shower model, estimate the number of positrons produced after 15 cm. (b) What is the average positron energy? (c) At what depth in the stack will the number of particles in the shower reach a maximum? (d) What is the maximum number of particles present in the shower?

3. (a) Estimate the total depth of a practical 15 GeV electromagnetic calorimeter if we allow an additional $2t_{\max}$ beyond the shower maximum to minimise the probability of escaping particles. (b) How does this compare with the total depth of a 15 GeV hadron calorimeter?

4. (a) Show that the minimum opening angle of the two photons in π^0 decay is $2m_\pi/E_\pi$, where E_π is the π^0 energy. (b) Assume that the two-photon showers can be resolved if they are separated by two Moliere radii. Estimate the maximum π^0 energy that can be resolved using a practical lead-scintillator calorimeter 2 m from the interaction point.

Bibliography

[1] U. Amaldi, "Fluctuations in Calorimetry Measurements", Physica Scripta **23** (1981) 409-424.

[2] C. Fabjan, "Calorimetry in High-Energy Physics", Techniques and Concepts of High Energy Physics-III, T. Ferbel, ed. (Plenum Pub. Corp. 1985).

[3] R.C. Fernow, "Introduction to experimental particle physics", Cambridge University Press (1986).

[4] K. Kleinknecht, "Particle Detectors", Phys. Reports **84** (1982) 85-161.

[5] G.E. Knoll, "Radiation Detection and Measurement", John Wiley and Sons (1989).

[6] W.R. Leo, "Techniques for Nuclear and Particle Physics Experiments", Springer-Verlag, (1987).

[7] K. Nakamura *et al.* (Particle Data Group), "The Review of Particle Physics", J. Phys. G **37**, 075021 (2010).